Figure 6. Defects in myotube formation in C2C12 cells caused by overexpression of LARGE. (**A**) C2C12 cells were transfected with LARGE, and two stable transfectants, clones 1 and 2, were obtained. On western blotting analysis with antibody against the N-terminal domain of LARGE (LARGE-N), clone 1 migrated at 75 kDa (white arrow), whereas clone 2 migrated at 90 kDa (black arrow) in both myoblast and myotube. Using antibody against the C-terminus of LARGE (LARGE-C), clone 2 migrated at 90 kDa (black arrow), whereas clone 1 was not detected. The asterisk represents a nonspecific reaction of antibody. IIH6 antibody recognized hyperglycosylated α-DG at 130–250 kDa in clone 2, whereas, in clone 1, IIH6 detected a fainter band at a lower position than in the control, indicating hypoglycosylated α-DG. Glyceraldehyde-3-phosphate dehydrogenase (GAPDH) was used as an internal control. (**B**) Cell numbers of clones 1 and 2 of the C2C12 myoblast were significantly less than those of the control 2 days after plating, indicating suppressed proliferation. *P* < 0.001 is represented by ***. (**C**) C2C12 myoblasts were allowed to form myotubes by switching the growth medium to differentiation medium. Vigorous myotube formation was observed in both control and clone 1; however, smaller myotubes were only occasionally observed in clone 2. Scale bar represents 100 μm. (**D**) The fusion index of clone 2 was significantly lower than that of the control and clone 1. NS = not statistically significant. *P* < 0.001 is represented by ***.

the defective myoblast fusion caused by the overexpression of LARGE.

DISCUSSION

The interaction between α-DG and laminin plays a critical role in stabilizing the sarcolemma against muscle contraction. Disruption of this linkage results in a high susceptibility to contraction-induced damage, eventually followed by muscular cell degeneration. This mechanism is hypothesized to underlie the pathogenesis of dystroglycanopathy (12). In the case of laminin α2 chain-deficient MDC1A, the main cause of muscle cell degeneration seems to be a defect in polymerization of laminin-211; however, in some cases where mutations reside in the G domain of laminin α2, the defective interaction of laminin with α-DG may also play an important role (37,39,42). LARGE is a glycosyltransferase that catalyzes addition of the repeating disaccharide -3Xylα1-3GlcUAβ1- to the *O*-mannosyl glycan of α-DG (10). Because LARGE facilitates the glycosylation of α-DG and highly enhances its laminin-binding activity irrespective of the gene involved (38), the overexpression of

LARGE is considered one of the most promising possible therapies for muscular dystrophies such as dystroglycanopathy and MDC1A. In the present study, we generated transgenic mice that overexpress LARGE to evaluate the effects on skeletal muscles. To date, several LARGE transgenic mouse lines have been reported. First, Brockington *et al.* reported LARGE Tg mouse lines, in which the CAG promoter drove the expression of LARGE, exhibited hyperglycosylation of α-DG in skeletal and cardiac muscles but not in the brain, kidneys, liver or intestines (48). A second mouse line described by Gumerson *et al.* expressed LARGE under control of the MCK promoter, and α-DG was hyperglycosylated in the skeletal and cardiac muscles (49). In contrast to these transgenic lines, our LARGE Tg mouse exhibits hyperglycosylation of α-DG widely in most tissues, including skeletal and cardiac muscles, the brain, peripheral nerves, kidney and liver. As dystroglycanopathy and MDC1A are multi-organ disorders involving brain, eye and peripheral nerves as well as skeletal and cardiac muscles, our LARGE Tg mouse represents a powerful tool to test the effect of overexpression of LARGE in these tissues.

Table 1. Change in gene expression relating to skeletal muscle regeneration, myoblast and satellite cell

Keyword	Symbol	Genbank accession	Description	Z-score	Ratio
Skeletal muscle regeneration	Igf1	NM_010512	Insulin-like growth factor 1 (Igf1), transcript variant 1	−2.42	0.33
	Igf1	NM_184052	Insulin-like growth factor 1 (Igf1), transcript variant 2	−2.59	0.31
Myoblast	Thbs4	NM_011582	Thrombospondin 4 (Thbs4)	3.43	4.07
	Itgb1bp3	NM_027120	Integrin beta 1 binding protein 3 (Itgb1bp3)	3.23	3.56
	Thbs4	NM_011582	Thrombospondin 4 (Thbs4)	2.75	2.95
	Plg	NM_008877	Plasminogen (Plg)	2.23	15.10
	Neo1	AK052439	13-day embryo lung cDNA, RIKEN full-length enriched library, clone:D430023D05	2.02	11.48
	Casp1	NM_009807	Caspase 1 (Casp1)	−2.05	0.31
	Igf1	NM_010512	Insulin-like growth factor 1 (Igf1), transcript variant 1	−2.42	0.33
	Igf1	NM_184052	Insulin-like growth factor 1 (Igf1), transcript variant 2	−2.59	0.31
	Btg1	NM_007569	B-cell translocation gene 1, anti-proliferative (Btg1)	−2.76	0.33
Satellite cell	Igf1	NM_010512	Insulin-like growth factor 1 (Igf1), transcript variant 1	−2.42	0.33
	Igf1	NM_184052	Insulin-like growth factor 1 (Igf1), transcript variant 2	−2.59	0.31

We crossed the LARGE Tg mice with two distinct mouse models, dy^{2J} and *FKTN* cKO mice, the former is a model for MDC1A and the latter for FCMD (39,40). Contrary to expectations, the muscular dystrophy was worsened in both mouse models. The features of the worsened phenotype was common to these two lines and characterized by decreased or unchanged central nucleation and reduced diameter of muscle fibers, suggesting the insufficiently activated regeneration. Because fibrosis is a result of muscle fiber necrosis, regeneration should be activated to replace the damaged tissue. However, in both dy^{2J}/LARGE and *FKTN* cKO/LARGE mice, the central nucleation was not accelerated and the diameter of myofibers remained small, suggesting that the regeneration was insufficiently activated. Very recently, Whitmore *et al.* have reported that the muscular dystrophy of $FKRP_{MD}$ mouse, a model of another dystroglycanopathy (LGMD2I), was exacerbated when these mice were crossed with their LARGE Tg mice. However, they did not investigate the cause leading to the worsened muscular dystrophy in these mice (50). The present report is the first to describe that the worsened phenotype is related to the defective regeneration of skeletal muscle.

To gain further insight into the regeneration process in dy^{2J}/LARGE and *FKTN* cKO/LARGE mice, we assessed satellite cells and regenerating fibers in these mice. Satellite cells are muscle stem cells located in a niche on the surface of myofiber beneath the ensheathing basement membrane (51). Upon activation, they rapidly generate myoblasts. After proliferation and migration, the myoblasts further differentiate and eventually fuse together to form myotubes (51,52). We labeled the satellite cells with M-cadherin and the regenerating fibers with embryonic MyHC. Because M-cadherin stains satellite cells and actively proliferating myoblasts, whereas embryonic MyHC stains newly formed myotubes, immunolabeling of the former reflects an early stage and the latter a late stage of regeneration (44,52). However, neither the M-cadherin-positive cells nor the embryonic MyHC-positive myofibers were consistently increased in either the dy^{2J}/LARGE or the *FKTN* cKO/LARGE mice. These should increase if the regeneration process proceeds properly (44,45). Therefore, our findings provide strong evidence that both the early and the late stage of regeneration are impaired in dy^{2J}/LARGE and *FKTN* cKO/LARGE mice. The embryonic MyHC-stained area was slightly increased in *FKTN* cKO/LARGE

mice. This may be accounted for by the existence of a limit of regeneration, which was exceeded in dy^{2J}/LARGE mice but not in *FKTN* cKO/LARGE mice. In a previous study, we injected cardiotoxin into LARGE Tg mice to induce an acute muscle injury and observed a reduction in muscle fiber diameter as compared with controls, suggesting a defect in myoblast fusion (41). Our current data are consistent with this observation and further support the notion that the overexpression of LARGE results in suppression of the skeletal muscle regeneration, regardless of whether the involved injury is acute or chronic.

Prompted by these results, we further examined whether the overexpression of LARGE affects the myotube formation of C2C12 cells, an established *in vitro* model for the muscle regeneration. In agreement with the data obtained using model mice, the overexpression of LARGE in C2C12 cells led to defects in both proliferation and fusion of myoblasts. The proliferation and fusion of C2C12 cells represent the early and the late stage of the myotube formation, and the overexpression of LARGE affected these both stages. This recapitulates the defect in the muscle regeneration of mice where both the M-cadherin-positive satellite cells (early stage) and the embryonic MyHC-labeled newly fused myotubes (late stage) were affected. Interestingly, the clone 1 of C2C12 cells, in which α-DG was hypoglycosylated, exhibited suppressed proliferation, but normal fusion of myoblasts. In a previous paper, we showed that the coordinated up-regulation of LARGE and the extension of the repeating disaccharides on α-DG are necessary for adequate muscle regeneration (41). In the present study, we provide the first data showing that both the hypo- and hyperglycosylation of α-DG result in defective regeneration, the former by suppressing myoblast proliferation and the latter by reducing proliferation and fusion of myoblasts.

To dissect the mechanism underlying the suppression of regeneration by LARGE, we conducted a DNA microarray analysis and identified a significant reduction in the expression of IGF-1. This reduction was confirmed at the protein level both in LARGE Tg mice and clone 2 of C2C12 cells. IGF-1 is an autocrine/paracrine peptide growth factor with primary roles in promoting myoblast proliferation, differentiation to myofibers and the hypertrophy of skeletal muscles (47). Muscle injury up-regulates the expression of IGF-1 by satellite cells, and after secretion, it binds to the IGF-1 receptors on the muscle
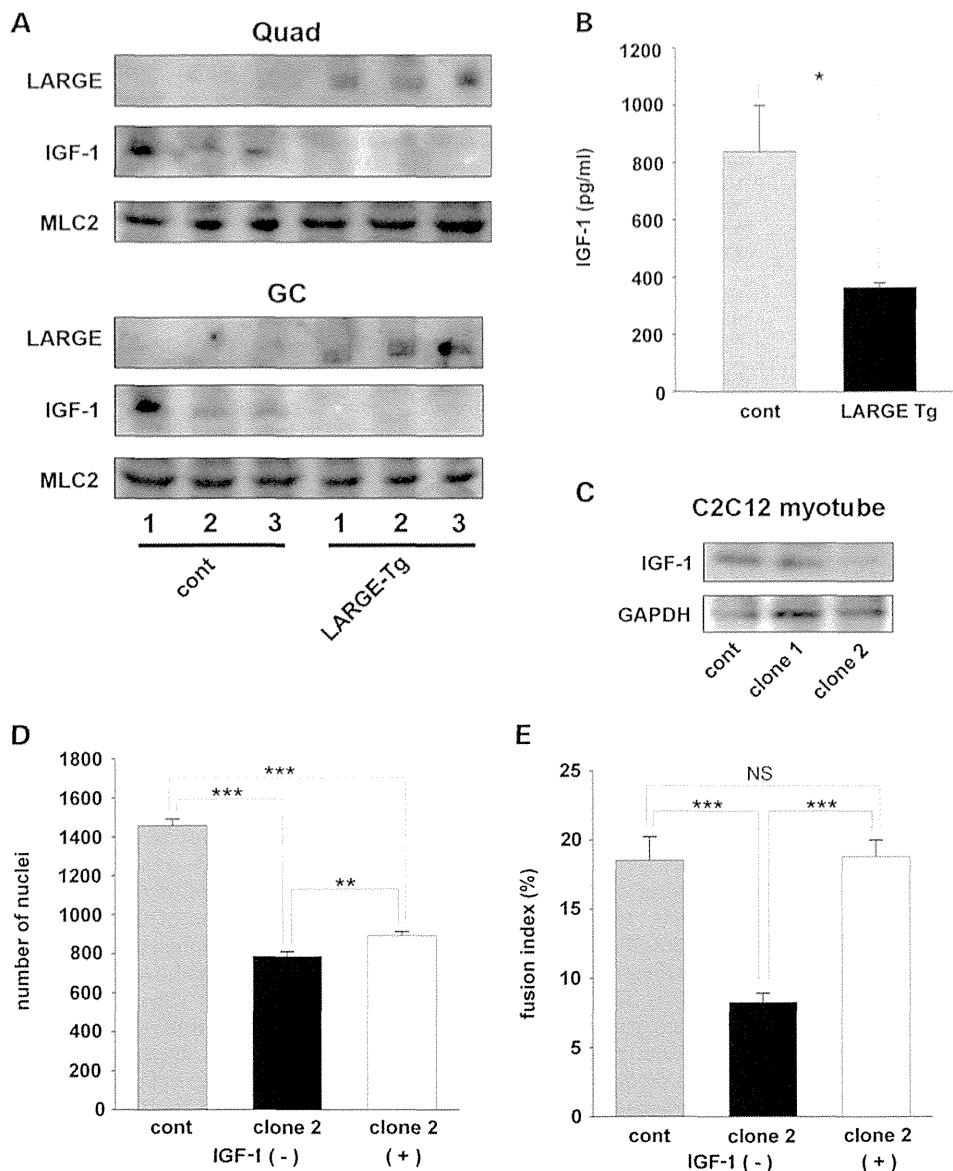
Figure 7. Reduced expression of IGF-1 by overexpression of LARGE and restoration of C2C12 myoblast fusion by IGF-1 supplementation. (**A**) Western blotting analysis demonstrated that expression of IGF-1 was reduced in both quadriceps and gastrocnemius muscles of LARGE Tg mice as compared with the controls ($n = 3$ of each strain). Myosin light chain 2 (MLC2) was used as an internal control. (**B**) Quantitative measurements by ELISA revealed that IGF-1 was significantly decreased in the skeletal muscle of LARGE Tg mice ($n = 3$, for all genotypes). $P < 0.05$ is represented by *. (**C**) Western blotting showed that expression of IGF-1 in C2C12 myotube was reduced in clone 2 but not in clone 1, indicating that the reduction of IGF-1 is associated with hyperglycosylation of α-DG. Glyceraldehyde-3-phosphate dehydrogenase (GAPDH) was used as an internal control. (**D**) Clone 2 of C2C12 myoblasts was supplemented with IGF-1 and allowed to differentiate into myotubes. Counting nuclei at 6 days after plating revealed that the number of nuclei in the IGF-1-treated clone 2 was slightly increased as compared with the untreated clone, whereas it was significantly less than that of the control. (**E**) The fusion index of IGF-1-treated clone 2 was markedly increased and exhibited no significant difference from the control. NS = not statistically significant. $^*P < 0.05$, $^{**}P < 0.01$ and $^{***}P < 0.001$.

cell surface (47). Transgenic overexpression of IGF-1 in mice demonstrated the maintained regeneration efficacy in aged mice and the reduced muscle pathology in dystrophic mice (53–55). Remarkably, the supplementation of IGF-1 fully restored the fusion of myoblasts in C2C12 cells, implying that the impaired fusion of myoblasts was caused, at least partially, via the reduced expression of IGF-1. In the present study, the number of C2C12 nuclei was not restored after the supplementation of IGF-1. The IGF-1 supplementation favors proliferation of myoblasts in some cases and facilitates myotube formation in others, depending on its concentration and the timing of the supplementation (56,57). This biphasic effect of IGF-1 may explain why the number of nuclei was not fully rescued in the C2C12 cells.

The mechanism leading to the reduction of IGF-1 expression by the overexpression of LARGE is still unclear. One possibility is that alteration of the signal transduction through DG might affect the expression of IGF-1. It is known that a tyrosine residue in the C-terminal PPxY motif of β-DG is phosphorylated in an adhesion-dependent manner (58). This phosphorylation regulates the interaction of β-DG with dystrophin, utrophin and SH2 domain-containing signaling proteins (58–60). Moreover, the interaction of laminin with α-DG propagates signals through the PI3K/AKT and Rac1/JNK pathways (61,62). The increased interaction of laminin with α-DG by LARGE may alter these or still unknown signaling pathway and eventually affect the expression of IGF-1. Another possibility is that unidentified proteins other than α-DG might be modified by LARGE and cause the alteration of the IGF-1 expression (63). Finally, it should be considered that factors or processes unrelated to decreased IGF-1 expression might also contribute to the regeneration defect. It has been shown that the interaction of α-DG with laminin inhibits the migration of cultured cells by attenuating the integrin signal that activates the ERK/AKT pathway (64). As myoblasts must migrate to the damaged site during muscle regeneration (51,52), increased glycosylation by LARGE might suppress regeneration by inactivating this pathway. In addition, mechanisms not involving muscle regeneration might also underlie the worsened muscular dystrophy especially in *FKTN* cKO/LARGE mice, in which the regeneration defect was not so striking as dy^{2J}/LARGE mice.

In conclusion, we generated LARGE Tg mice and crossed them with dy^{2J} and *FKTN* cKO mice to investigate the effect of overexpression of LARGE. In both resulting strains, the muscular dystrophy was worsened. We identified suppressed muscle regeneration, which at least partially resulted from the reduced IGF-1 expression, as the cause of the deterioration seen in muscular dystrophy. In our study, as well as others (50), the transgenic overexpression of LARGE led to the exacerbation of muscular dystrophy, whereas adeno-associated virus-mediated transfer of LARGE has been reported to ameliorate the phenotype of muscular dystrophy in LARGE^{myd} and POMGnT1 KO mice (65). Although the reason for this discrepancy remains unclear, the expression level, timing of expression and/or transduced cell type may be different between these two gene delivery systems. In order to develop a therapeutic strategy using the overexpression of LARGE, its adverse effects on skeletal muscle should be carefully investigated.

MATERIALS AND METHODS

Generation of mice

Generation of LARGE Tg mice and MCK-fukutin conditional knockout mice (*FKTN* cKO mice) were reported previously (40,41). B6.WK-*Lama2dy-2J*/J (Dy^{2J}) mice were obtained from Jackson laboratory (Bar Harbor, Maine, USA). Mice heterozygous for the *Lama2dy-2J* mutation were crossed with mice hemizygous for LARGE Tg, and mice heterozygous for *Lama2dy-2J* carrying LARGE were further crossed with mice heterozygous for *Lama2dy-2J* to generate mice homozygous for *Lama2dy-2J* carrying LARGE hemizygously (Dy^{2J}/LARGE). To generate *FKTN* cKO/LARGE mice, we first crossed heterozygous $FKTN^{lox/+}$ mice carrying MCK-Cre

hemizygously with mice hemizygous for LARGE Tg. Then, $FKTN^{lox/+}$ mice carrying both MCK-Cre Tg and LARGE Tg were crossed with homozygous $FKTN^{lox/lox}$ mice to obtain $FKTN^{lox/lox}$ mice carrying both MCK-Cre Tg and LARGE Tg hemizygously (*FKTN* cKO/LARGE). Genotyping of $FKTN^{lox}$, MCK-Cre Tg and LARGE Tg was performed using PCR. To identify the single base substitution in the *Lama2dy-2J* allele, we used DNA sequencing. The experiments were approved by the living modified organism safety committee and animal ethics committee of Teikyo University School of Medicine, and the mice were maintained in accordance with the animal care guideline of Teikyo University School of Medicine.

Antibodies

Rabbit polyclonal antibodies against 40 amino acids in the N-terminal domain (a.a. 61–100) and 31 amino acids in the C-terminal domain (a.a. 726–756) of human LARGE were generated (Supplementary Material, Fig. S4A). Goat polyclonal antibody, GT20ADG, against core protein of α-DG (12) was a kind gift from Dr K. P. Campbell (University of Iowa, Iowa City, Iowa, USA). In addition, the following antibodies were used in this study: mouse monoclonal antibody IIH6 against glycosylated α-DG (Millipore), rabbit polyclonal antibody against C-terminal domain of β-DG (Sigma–Aldrich), rabbit polyclonal antibody against EHS-laminin (Sigma–Aldrich), rat monoclonal antibody against laminin α2 chain (Enzo), rat monoclonal antibody against laminin β1 chain (Millipore), rat monoclonal antibody against laminin γ1 chain (Millipore), rabbit polyclonal antibody against M-cadherin (Life Technologies), goat polyclonal antibody against IGF-1 (R&D systems), mouse monoclonal antibody against FLAG (Sigma–Aldrich), mouse monoclonal antibody against α-actinin (Sigma–Aldrich), rabbit polyclonal antibody against GAPDH (Santa Cruz Biotechnology), mouse monoclonal antibody F1.653 against embryonic MyHC (Developmental Studies Hybridoma Bank), mouse monoclonal antibody MF-20 against MyHC (Developmental Studies Hybridoma Bank), Alexafluor 488- and 594-conjugated secondary antibodies (Life Technologies) and horseradish peroxidase-labeled secondary antibodies (GE Healthcare).

Histology, immunofluorescence and electron microscopy

Histological and immunofluorescent microscopic analysis was performed on Dy^{2J}, Dy^{2J}/LARGE, *FKTN* cKO, *FKTN* cKO/LARGE and their age-matched control mice between the ages 8 to 27 weeks. Muscles were removed and frozen in liquid nitrogen-cooled isopentane, and cryosections of 8 μm in thickness were prepared. The standard technique was used for hematoxylin–eosin (H-E) staining. For immunofluorescence analysis, the sections were blocked with 5% bovine serum albumin in phosphate-buffered saline (PBS), followed by incubation with primary antibodies for 1 h and then incubated with Alexafluor 488- or 594-conjugated secondary antibody for 1 h. Subsequently, the sections were mounted with Vectashield (Vector Laboratories) and observed under a FSX100 fluorescence microscope (Olympus) or a confocal laser microscope A1 (Nikon). For immunofluorescent analyses of C2C12 cells, myoblasts and myotubes were fixed in 4% paraformaldehyde,

permeabilized with 0.2% Triton X-100 and stained with anti-MyHC for 1 h using a mouse on mouse (M.O.M.) kit (Vector Laboratories). After washing with PBS, the cells were incubated for 30 min with Alexafluor 488-conjugated anti-mouse IgG antibody. The slides were mounted with Vectashield with DAPI (Vector Laboratories), and the fluorescent images were taken using a FSX100 fluorescence microscope (Olympus). The basement membranes of the quadriceps muscles were observed with a transmission electron microscopy H-7650 (Hitachi High-technologies) using the standard techniques. The *in situ* ligand overlay assay was described elsewhere (66).

Cell culture and transfection

C2C12 cells were obtained from ATCC and HEK293 cells from the Human Science Research Resource Bank (Osaka, Japan). C2C12 myoblasts were plated at a density of 1.9×10^6/ml on poly-D-lysine/laminin-coated coverslips (Corning) and grown in Dulbecco's modified Eagle's medium supplemented with 10% fetal bovine serum (ATCC), 100 U/ml penicillin G and 100 µg/ml streptomycin (Life Technologies) (growth medium). Next day, cells were induced to differentiate into myotubes by lowering the serum concentration to 2% horse serum (differentiation medium). Five days after replacing the medium, cells were stained for immunofluorescent analysis or harvested for biochemical assay. In some experiments, 10 ng/ml of mouse recombinant IGF-1 (Cell Signaling Technology) was added to both the growth and the differentiation mediums. HEK293 cells were plated on plastic culture dishes (DB Bioscience) and grown in the growth medium described earlier. All cells were grown in a humidified 37°C incubator with 5% CO_2 and 95% air. Human LARGE cDNA was obtained from OriGene and cloned into pCMV-FLAG-MAT-Tag-2 (Sigma–Aldrich) for transient transfection of cells. C2C12 and HEK293 cells were transfected using Effectene (Qiagen). For stable transfection of C2C12 cells, the CAG promoter and human LARGE cDNA were cloned into pLenti6/R4R2/V5-DEST using Gateway BP reaction and lentivirus expression vector was generated according to the standard protocol. Stable transfectants were selected in growth medium supplemented with 2.5 µg/ml of Blasticidin S (Life Technologies). Expression vectors for the deletion and chimeric mutants of human LARGE were constructed using the KOD-Plus-Mutagenesis Kit according to the manufacturer's protocols (Toyobo).

Morphometric analysis

For morphometric analysis of skeletal muscles, 5×5 stitching images of gastrocnemius muscles, captured at a magnification of 20× using a FSX100 fluorescence microscope (Olympus), were used. Three mice from each genotype were analyzed ($n = 3$), at ages of 16–22 weeks for dy^{2J}, dy^{2J}/LARGE mice and their controls and 24–27 weeks for *FKTN* cKO, *FKTN* cKO/LARGE mice and their controls. For the evaluation of fibrosis, the area stained by anti-mouse IgG, which nonspecifically labels connective tissues and fibrosis, was quantitatively measured by the ImageJ software. For assessment of size variation in muscle fibers, minimal Feret's diameter of individual muscle fiber stained by anti-laminin α2 was measured using ImageJ software. For quantitative evaluation of centrally

located nuclei, the total nuclei number was counted using ImageJ software and internal nuclei were assessed by visual inspection of images double-stained by anti-laminin α2 and DAPI. Satellite cells stained by M-cadherin located just beneath the basement membrane labeled with anti-laminin α2 were counted. Regenerating fibers were immunolabeled by embryonic MyHC, and the area was measured using ImageJ software. For morphometric analysis of C2C12 cells, 5×5 stitching images of at least five visual fields were captured at a magnification of 20×. Number of DAPI-stained nuclei was counted with ImageJ software, and the fusion index was calculated by dividing the nuclei number in MyHC-stained cells by total nuclei number. The same experiment was repeated three times. Statistical differences were evaluated by *t*-test, and *P*-values < 0.05 were considered statistically significant.

Western blotting, blot overlay assay and ELISA

For western blotting and laminin blot overlay assay, tissues were isolated and disrupted with a polytron followed by Dounce homogenization in 50 mM Tris–HCl, pH 7.4, 150 mM NaCl, 0.6 mg/ml pepstatin A, 0.5 mg/ml leupeptin, 0.5 mg/ml aprotinin, 0.75 mM benzamidine and 0.1 mM PMSF. Proteins were then extracted by boiling in sample buffer (65 mM Tris–HCl, pH 7.4, 0.115 M sucrose, 3% SDS, 1% β-mercaptoethanol) for 3 min. After briefly spinning down debris, the homogenate was applied to 4–15% SDS–PAGE. In some experiments, dissected skeletal muscles were homogenized and then incubated with 1% Triton X-100 to solubilize the membrane proteins, and α-DG was enriched by WGA (*wheat germ agglutinin*) chromatography. Western blotting and laminin blot overlay assay was performed as described previously (12), and images were captured using LAS-3000 software (Fujifilm). For pH 12 extract overlay, skeletal muscles of dy^{2J} and control mice were homogenized, centrifuged at 35 000*g* for 20 min, and the pellets were incubated at pH 12 for 1 h and centrifuged at 140 000*g* for 35 min. The supernatant, which included endogenous laminin, was incubated with blots overnight, and the laminin bound to α-DG was detected with anti-laminin antibody. Mouse gastrocnemius muscles and C2C12 myotubes were homogenized as described earlier, centrifuged at 20 000*g* for 10 min, and the concentration of IGF-1 in the supernatant was measured using a Quantikine ELISA kit for Mouse/Rat IGF-1 (R&D Systems).

DNA microarray analysis

Gastrocnemius muscles of LARGE Tg mouse and control mouse at 16 weeks of age were dissected and stored in RNAlater (Life Technologies). Total RNA was isolated from the muscles using RNeasy Fibrous Tissue Midi Kit (Qiagen). Microarray analysis was performed using Whole Mouse Genome Oligo Microarray 4×44 k (Agilent Technologies). Microarray data were extracted from scanned images and analyzed using GeneSpring software (Agilent Technologies). Gene ontology search was performed within the genes that exhibited a significant change in expression, i.e. z-score ≥ 2 and ratio ≥ 1.5 (increase in LARGE Tg) or z-score ≤ -2 and ratio ≤ 0.66 (decrease in LARGE Tg).

Miscellaneous

Body weights of male and female dy^{2J}, dy^{2J}/LARGE and control mice ($n = 4–15$) were measured at 4 and 8 weeks of age. Grip strength was measured for 10 consecutive trials for dy^{2J}, dy^{2J}/LARGE and control mice ($n = 4–6$) at the age of 8 weeks using a grip strength meter (Panlab). Kaplan–Meier estimates of survival probabilities were calculated for dy^{2J} and dy^{2J}/LARGE mice ($n = 11$ and 15, respectively) using survival analysis add-on software to Excel (NAG).

SUPPLEMENTARY MATERIAL

Supplementary Material is available at *HMG* online.

ACKNOWLEDGEMENTS

FUNDING

REFERENCES

1. Ibraghimov-Beskrovnaya, O., Ervasti, J.M., Leveille, C.J., Slaughter, C.A., Sernett, S.W. and Campbell, K.P. (1992) Primary structure of dystrophin-associated glycoproteins linking dystrophin to the extracellular matrix. *Nature*, **355**, 696–702.
2. Sugita, S., Saito, F., Tang, J., Satz, J., Campbell, K.P. and Südhof, T.C. (2001) A stoichiometric complex of neurexins and dystroglycan in brain. *J. Cell Biol.*, **154**, 435–445.
3. Sato, S., Omori, Y., Katoh, K., Kondo, M., Kanagawa, M., Miyata, K., Funabiki, K., Koyasu, T., Kajimura, N., Miyoshim, T. *et al.* (2008) Pikachurin, a dystroglycan ligand, is essential for photoreceptor ribbon synapse formation. *Nat. Neurosci.*, **11**, 923–931.
4. Ervasti, J.M. and Campbell, K.P. (1993) A role for the dystrophin-glycoprotein complex as a transmembrane linker between laminin and actin. *J. Cell. Biol.*, **122**, 809–823.
5. Jung, D., Yang, B., Meyer, J., Chamberlain, J.S. and Campbell, K.P. (1995) Identification and characterization of the dystrophin anchoring site on β-dystroglycan. *J. Biol. Chem.*, **270**, 27305–27310.
6. Kanagawa, M., Saito, F., Kunz, S., Yoshida-Moriguchi, T., Barresi, R., Kobayashi, Y.M., Muschler, J., Dumanski, J.P., Michele, D.E., Oldstone, M.B. *et al.* (2004) Molecular recognition by LARGE is essential for expression of functional dystroglycan. *Cell*, **117**, 953–964.
7. Saito, F., Saito-Arai, Y., Nakamura, A., Shimizu, T. and Matsumura, K. (2008) Processing and secretion of the N-terminal domain of α-dystroglycan in cell culture media. *FEBS Lett.*, **582**, 439–444.
8. Chiba, A., Matsumura, K., Yamada, H., Inazu, T., Shimizu, T., Kusunoki, S., Kanazawa, I., Kobata, A. and Endo, T. (1997) Structures of sialylated O-linked oligosaccharides of bovine peripheral nerve α-dystroglycan. The role of a novel O-mannosyl-type oligosaccharide in the binding of α-dystroglycan with laminin. *J. Biol. Chem.*, **272**, 2156–2162.
9. Yoshida-Moriguchi, T., Yu, L., Stalnaker, S.H., Davis, S., Kunz, S., Madson, M., Oldstone, M.B., Schachter, H., Wells, L. and Campbell, K.P. (2010) O-mannosyl phosphorylation of α-dystroglycan is required for laminin binding. *Science*, **327**, 88–92.
10. Inamori, K., Yoshida-Moriguchi, T., Hara, Y., Anderson, M.E., Yu, L. and Campbell, K.P. (2012) Dystroglycan function requires xylosyl- and glucuronyltransferase activities of LARGE. *Science*, **335**, 93–96.
11. Yoshida-Moriguchi, T., Willer, T., Anderson, M.E., Venzke, D., Whyte, T., Muntoni, F., Lee, H., Nelson, S.F., Yu, L. and Campbell, K.P. (2013) SGK196 is a glycosylation-specific O-mannose kinase required for dystroglycan function. *Science*, **341**, 896–899.
12. Michele, D.E., Barresi, R., Kanagawa, M., Saito, F., Cohn, R.D., Satz, J.S., Dollar, J., Nishino, I., Kelley, R.I., Somer, H. *et al.* (2002) Post-translational disruption of dystroglycan-ligand interactions in congenital muscular dystrophies. *Nature*, **418**, 417–422.
13. Brown, S.C. and Winder, S.J. (2011) Dystroglycan and dystroglycanopathies: report of the 187th ENMC Workshop 11–13 November 2011, Naarden, The Netherlands. *Neuromuscul. Disord.*, **22**, 659–668.
14. Kobayashi, K., Nakahori, Y., Miyake, M., Matsumura, K., Kondo-Iida, E., Nomura, Y., Segawa, M., Yoshioka, M., Saito, K., Osawa, M. *et al.* (1998) An ancient retrotransposal insertion causes Fukuyama-type congenital muscular dystrophy. *Nature*, **394**, 388–392.
15. Taniguchi-Ikeda, M., Kobayashi, K., Kanagawa, M., Yu, C.C., Mori, K., Oda, T., Kuga, A., Kurahashi, H., Akman, H.O., DiMauro, S. *et al.* (2011) Pathogenic exon-trapping by SVA retrotransposon and rescue in Fukuyama muscular dystrophy. *Nature*, **478**, 127–131.
16. Beltran-Valero, D.B., Currier, S., Steinbrecher, A., Celli, J., van Beusekom, E., van der, Z.B., Kayserili, H., Merlini, L., Chitayat, D., Dobyns, W.B. *et al.* (2002) Mutations in the O-mannosyltransferase gene POMT1 give rise to the severe neuronal migration disorder Walker-Warburg syndrome. *Am. J. Hum. Genet.*, **71**, 1033–1043.
17. Manya, H., Chiba, A., Yoshida, A., Wang, X., Chiba, Y., Jigami, Y., Margolis, R.U. and Endo, T. (2004) Demonstration of mammalian protein O-mannosyltransferase activity: coexpression of POMT1 and POMT2 required for enzymatic activity. *Proc. Natl. Acad. Sci. USA*, **101**, 500–505.
18. van Reeuwijk, J., Janssen, M., van den, E.C., Beltran-Valero de, B.D., Sabatelli, P., Merlini, L., Boon, M., Scheffer, H., Brockington, M., Muntoni, F. *et al.* (2005) POMT2 mutations cause α-dystroglycan hypoglycosylation and Walker-Warburg syndrome. *J. Med. Genet.*, **42**, 907–912.
19. Yoshida, A., Kobayashi, K., Manya, H., Taniguchi, K., Kano, H., Mizuno, M., Inazu, T., Mitsuhashi, H., Takahashi, S., Takeuchi, M. *et al.* (2001) Muscular dystrophy and neuronal migration disorder caused by mutations in a glycosyltransferase, POMGnT1. *Dev. Cell*, **1**, 717–724.
20. Longman, C., Brockington, M., Torelli, S., Jimenez-Mallebrera, C., Kennedy, C., Khalil, N., Feng, L., Saran, R.K., Voit, T., Merlini, L. *et al.* (2003) Mutations in the human LARGE gene cause MDC1D, a novel form of congenital muscular dystrophy with severe mental retardation and abnormal glycosylation of α-dystroglycan. *Hum. Mol. Genet.*, **12**, 2853–2861.
21. Jae, L.T., Raaben, M., Riemersma, M., van Beusekom, E., Blomen, V.A., Velds, A., Kerkhoven, R.M., Carette, J.E., Topaloglu, H., Meinecke, P. *et al.* (2013) Deciphering the glycosylome of dystroglycanopathies using haploid screens for lassa virus entry. *Science*, **340**, 479–483.
22. Manzini, M.C., Tambunan, D.E., Hill, R.S., Yu, T.W., Maynard, T.M., Heinzen, E.L., Shianna, K.V., Stevens, C.R., Partlow, J.N., Barry, B.J. *et al.* (2012) Exome sequencing and functional validation in zebrafish identify GTDC2 mutations as a cause of Walker-Warburg syndrome. *Am. J. Hum. Genet.*, **91**, 541–547.
23. Stevens, E., Carss, K.J., Cirak, S., Foley, A.R., Torelli, S., Willer, T., Tambunan, D.E., Yau, S., Brodd, L., Sewry, C.A. *et al.* (2013) Mutations in B3GALNT2 cause congenital muscular dystrophy and hypoglycosylation of α-dystroglycan. *Am. J. Hum. Genet.*, **92**, 354–365.
24. Lefeber, D.J., de Brouwer, A.P., Morava, E., Riemersma, M., Schuurs-Hoeijmakers, J.H., Absmanner, B., Verrijp, K., van den Akker, W.M., Huijben, K., Steenbergen, G. *et al.* (2011) Autosomal recessive dilated cardiomyopathy due to DOLK mutations results from abnormal dystroglycan O-mannosylation. *PLoS. Genet.*, **7**, e1002427.
25. Carss, K.J., Stevens, E., Foley, A.R., Cirak, S., Riemersma, M., Torelli, S., Hoischen, A., Willer, T., van, S.M., Moore, S.A. *et al.* (2013) Mutations in

GDP-mannose pyrophosphorylase B cause congenital and limb-girdle muscular dystrophies associated with hypoglycosylation of α-dystroglycan. *Am. J. Hum. Genet.*, **93**, 29–41.

26. Yang, A.C., Ng, B.G., Moore, S.A., Rush, J., Waechter, C.J., Raymond, K.M., Willer, T., Campbell, K.P., Freeze, H.H. and Mehta, L. (2013) Congenital disorder of glycosylation due to DPM1 mutations presenting with dystroglycanopathy-type congenital muscular dystrophy. *Mol. Genet. Metab.*, **10**, 345–351.

27. Barone, R., Aiello, C., Race, V., Morava, E., Foulquier, F., Riemersma, M., Passarelli, C., Concolino, D., Carella, M., Santorelli, F. *et al.* (2012) DPM2-CDG: a muscular dystrophy-dystroglycanopathy syndrome with severe epilepsy. *Ann. Neurol.*, **72**, 550–558.

28. Lefeber, D.J., Schonberger, J., Morava, E., Guillard, M., Huyben, K.M., Verrijp, K., Grafakou, O., Evangeliou, A., Preijers, F.W., Manta, P. *et al.* (2009) Deficiency of Dol-P-Man synthase subunit DPM3 bridges the congenital disorders of glycosylation with the dystroglycanopathies. *Am. J. Hum. Genet.*, **85**, 76–86.

29. Brockington, M., Blake, D.J., Prandini, P., Brown, S.C., Torelli, S., Benson, M.A., Ponting, C.P., Estournet, B., Romero, N.B., Mercuri, E. *et al.* (2001) Mutations in the fukutin-related protein gene (FKRP) cause a form of congenital muscular dystrophy with secondary laminin α2 deficiency and abnormal glycosylation of α-dystroglycan. *Am. J. Hum. Genet.*, **69**, 1198–1209.

30. Buysse, K., Riemersma, M., Powell, G., van, R.J., Chitayat, D., Roscioli, T., Kamsteeg, E.J., van den Elzen, C., van, B.E., Blaser, S. *et al.* (2013) Missense mutations in β-1,3-*N*-acetylglucosaminyltransferase 1 (B3GNT1) cause Walker-Warburg syndrome. *Hum. Mol. Genet.*, **22**, 1746–1754.

31. Willer, T., Lee, H., Lommel, M., Yoshida-Moriguchi, T., de Bernabe, D.B., Venzke, D., Cirak, S., Schachter, H., Vajsar, J., Voit, T. *et al.* (2012) ISPD loss-of-function mutations disrupt dystroglycan O-mannosylation and cause Walker-Warburg syndrome. *Nat. Genet.*, **44**, 575–580.

32. Roscioli, T., Kamsteeg, E.J., Buysse, K., Maystadt, I., van Reeuwijk, J., van den Elzen, C., van Beusekom, E., Riemersma, M., Pfundt, R., Vissers, L.E. *et al.* (2012) Mutations in ISPD cause Walker-Warburg syndrome and defective glycosylation of α-dystroglycan. *Nat. Genet.*, **44**, 581–585.

33. Vuillaumier-Barrot, S., Bouchet-Seraphin, C., Chelbi, M., Devisme, L., Quentin, S., Gazal, S., Laquerriere, A., Fallet-Bianco, C., Loget, P., Odent, S. *et al.* (2012) Identification of mutations in TMEM5 and ISPD as a cause of severe cobblestone lissencephaly. *Am. J. Hum. Genet.*, **91**, 1135–1143.

34. Hara, Y., Balci-Hayta, B., Yoshida-Moriguchi, T., Kanagawa, M., Beltrán-Valero de Bernabé, D., Gündeşli, H., Willer, T., Satz, J.S., Crawford, R.W., Burden, S.J. *et al.* (2011) A dystroglycan mutation associated with limb-girdle muscular dystrophy. *N. Engl. J. Med.*, **364**, 939–946.

35. Muntoni, F. and Voit, T. (2004) The congenital muscular dystrophies in 2004: a century of exciting progress. *Neuromuscul. Disord.*, **14**, 635–649.

36. Helbling-Leclerc, A., Zhang, X., Topaloglu, H., Cruaud, C., Tesson, F., Weissenbach, J., Tomé, F.M., Schwartz, K., Fardeau, M., Tryggvason, K. *et al.* (1995) Mutations in the laminin α2-chain gene (LAMA2) cause merosin-deficient congenital muscular dystrophy. *Nat. Genet.*, **11**, 216–218.

37. Geranmayeh, F., Clement, E., Feng, L.H., Sewry, C., Pagan, J., Mein, R., Abbs, S., Brueton, L., Childs, A.M., Jungbluth, H. *et al.* (2010) Genotype-phenotype correlation in a large population of muscular dystrophy patients with LAMA2 mutations. *Neuromuscul. Disord.*, **20**, 241–250.

38. Barresi, R., Michele, D.E., Kanagawa, M., Harper, H.A., Dovico, S.A., Satz, J.S., Moore, S.A., Zhang, W., Schachter, H., Dumanski, J.P. *et al.* (2004) LARGE can functionally bypass α-dystroglycan glycosylation defects in distinct congenital muscular dystrophies. *Nat. Med.*, **10**, 696–703.

39. Sunada, Y., Bernier, S.M., Utani, A., Yamada, Y. and Campbell, K.P. (1995) Identification of a novel mutant transcript of laminin α2 chain gene responsible for muscular dystrophy and dysmyelination in dy^{2J} mice. *Hum. Mol. Genet.*, **4**, 1055–1061.

40. Kanagawa, M., Yu, C.C., Ito, C., Fukada, S., Hozoji-Inada, M., Chiyo, T., Kuga, A., Matsuo, M., Sato, K., Yamaguchi, M. *et al.* (2013) Impaired viability of muscle precursor cells in muscular dystrophy with glycosylation defects and amelioration of its severe phenotype by limited gene expression. *Hum. Mol. Genet.*, **22**, 3003–3015.

41. Goddeeris, M.M., Wu, B., Venzke, D., Yoshida-Moriguchi, T., Saito, F., Matsumura, K., Moore, S.A. and Campbell, K.P. (2013) LARGE glycans on dystroglycan function as a tunable matrix scaffold to prevent dystrophy. *Nature*, **503**, 136–140.

42. Colognato, H. and Yurchenco, P.D. (1999) The laminin α2 expressed by dystrophic dy(2J) mice is defective in its ability to form polymers. *Curr. Biol.*, **9**, 1327–1330.

43. Straub, V., Rafael, J.A., Chamberlain, J.S. and Campbell, K.P. (1997) Animal models for muscular dystrophy show different patterns of sarcolemmal disruption. *J. Cell. Biol.*, **139**, 375–385.

44. Irintchev, A., Zeschnigk, M., Starzinski-Powitz, A. and Wernig, A. (1994) Expression pattern of M-cadherin in normal, denervated, and regenerating mouse muscles. *Dev. Dyn.*, **199**, 326–337.

45. Kottlors, M. and Kirschner, J. (2010) Elevated satellite cell number in Duchenne muscular dystrophy. *Cell Tissue Res.*, **340**, 541–548.

46. Brockington, M., Torelli, S., Prandini, P., Boito, C., Dolatshad, N.F., Longman, C., Brown, S.C. and Muntoni, F. (2005) Localization and functional analysis of the LARGE family of glycosyltransferases: significance for muscular dystrophy. *Hum. Mol. Genet.*, **14**, 657–665.

47. Clemmons, D.R. (2009) Role of IGF-1 in skeletal muscle mass maintenance. *Trends Endocrinol. Metab.*, **20**, 349–356.

48. Brockington, M., Torelli, S., Sharp, P.S., Liu, K., Cirak, S., Brown, S.C., Wells, D.J. and Muntoni, F. (2010) Transgenic overexpression of LARGE induces α-dystroglycan hyperglycosylation in skeletal and cardiac muscle. *PLoS One*, **5**, e14434.

49. Gumerson, J.D., Davis, C.S., Kabaeva, Z.T., Hayes, J.M., Brooks, S.V. and Michele, D.E. (2013) Muscle-specific expression of LARGE restores neuromuscular transmission deficits in dystrophic LARGE^{myd} mice. *Hum. Mol. Genet.*, **22**, 757–768.

50. Whitmore, C., Fernandez-Fuente, M., Booler, H., Parr, C., Kavishwar, M., Ashraf, A., Lacey, E., Kim, J., Terry, R., Ackroyd, M.R. *et al.* (2014) The transgenic expression of LARGE exacerbates the muscle phenotype of dystroglycanopathy mice. *Hum. Mol. Genet.*, **23**, 1842–1855.

51. Relaix, F. and Zammit, P.S. (2012) Satellite cells are essential for skeletal muscle regeneration: the cell on the edge returns centre stage. *Development*, **139**, 2845–2856.

52. Ciciliot, S. and Schiaffino, S. (2010) Regeneration of mammalian skeletal muscle. Basic mechanisms and clinical implications. *Curr. Pharm. Des.*, **16**, 906–914.

53. Musarò, A., McCullagh, K., Paul, A., Houghton, L., Dobrowolny, G., Molinaro, M., Barton, E.R., Sweeney, H.L. and Rosenthal, N. (2001) Localized Igf-1 transgene expression sustains hypertrophy and regeneration in senescent skeletal muscle. *Nat. Genet.*, **27**, 195–200.

54. Barton, E.R., Morris, L., Musaro, A., Rosenthal, N. and Sweeney, H.L. (2002) Muscle-specific expression of insulin-like growth factor I counters muscle decline in mdx mice. *J. Cell. Biol.*, **157**, 137–148.

55. Kumar, A., Yamauchi, J., Girgenrath, T. and Girgenrath, M. (2011) Muscle-specific expression of insulin-like growth factor 1 improves outcome in Lama2Dy-w mice, a model for congenital muscular dystrophy type 1A. *Hum. Mol. Genet.*, **20**, 2333–2343.

56. Coolican, S.A., Samuel, D.S., Ewton, D.Z., McWade, F.J. and Florini, J.R. (1997) The mitogenic and myogenic actions of insulin-like growth factors utilize distinct signaling pathways. *J. Biol. Chem.*, **272**, 6653–6662.

57. Tureckova, J., Wilson, E.M., Cappalonga, J.L. and Rotwein, P. (2001) Insulin-like growth factor-mediated muscle differentiation: collaboration between phosphatidylinositol 3-kinase-Akt-signaling pathways and myogenin. *J. Biol. Chem.*, **276**, 39264–39270.

58. James, M., Nuttall, A., Ilsley, J.L., Ottersbach, K., Tinsley, J.M., Sudol, M. and Winder, S.J. (2000) Adhesion-dependent tyrosine phosphorylation of β-dystroglycan regulates its interaction with utrophin. *J. Cell. Sci.*, **113**, 1717–1726.

59. Ilsley, J.L., Sudol, M. and Winder, S.J. (2001) The interaction of dystrophin with β-dystroglycan is regulated by tyrosine phosphorylation. *Cell Signal.*, **13**, 625–632.

60. Sotgia, F., Lee, H., Bedford, M.T., Petrucci, T., Sudol, M. and Lisanti, M.P. (2001) Tyrosine phosphorylation of β-dystroglycan at its WW domain binding motif, PPxY, recruits SH2 domain containing proteins. *Biochemistry*, **40**, 14585–14592.

61. Langenbach, K.J. and Rando, T.A. (2002) Inhibition of dystroglycan binding to laminin disrupts the PI3K/AKT pathway and survival signaling in muscle cells. *Muscle Nerve.*, **26**, 644–653.

62. Zhou, Y., Jiang, D., Thomason, D.B. and Jarrett, H.W. (2007) Laminin-induced activation of Rac1 and JNKp46 is initiated by Src family kinases and mimics the effects of skeletal muscle contraction. *Biochemistry*, **46**, 14907–14916.

63. Zhang, P. and Hu, H. (2012) Differential glycosylation of α-dystroglycan and proteins other than α-dystroglycan by like-glycosyltransferase. *Glycobiology*, **22**, 235–247.

64. Bao, X., Kobayashi, M., Hatakeyama, S., Angata, K., Gullberg, D., Nakayama, J., Fukuda, M.N. and Fukuda, M. (2009) Tumor suppressor function of laminin-binding α-dystroglycan requires a distinct β3-N-acetylglucosaminyltransferase. *Proc. Natl. Acad. Sci. USA*, **106**, 12109–12114.

65. Yu, M., He, Y., Wang, K., Zhang, P., Zhang, S. and Hu, H. (2013) Adeno-associated viral-mediated LARGE gene therapy rescues the muscular dystrophic phenotype in mouse models of dystroglycanopathy. *Hum. Gene. Ther.*, **24**, 317–330.

66. Saito, F., Masaki, T., Saito, Y., Nakamura, A., Takeda, S., Shimizu, T., Toda, T. and Matsumura, K. (2007) Defective peripheral nerve myelination and neuromuscular junction formation in fukutin-deficient chimeric mice. *J. Neurochem.*, **101**, 1712–1722.

:⊚:**PLOS** | ONE

Contribution of Dysferlin Deficiency to Skeletal Muscle Pathology in Asymptomatic and Severe Dystroglycanopathy Models: Generation of a New Model for Fukuyama Congenital Muscular Dystrophy

CrossMark

Motoi Kanagawa[1¶], Zhongpeng Lu[1¶], Chiyomi Ito[1], Chie Matsuda[2], Katsuya Miyake[3], Tatsushi Toda[1]*

1 Division of Neurology/Molecular Brain Science, Kobe University Graduate School of Medicine, Kobe, Japan, 2 Biomedical Research Institute, National Institute of Advanced Industrial Science and Technology, Tsukuba, Japan, 3 Department of Histology and Cell Biology, School of Medicine, Kagawa University, Ikenobe, Miki, Kagawa, Japan

Abstract

Defects in dystroglycan glycosylation are associated with a group of muscular dystrophies, termed dystroglycanopathies, that include Fukuyama congenital muscular dystrophy (FCMD). It is widely believed that abnormal glycosylation of dystroglycan leads to disease-causing membrane fragility. We previously generated knock-in mice carrying a founder retrotransposal insertion in *fukutin*, the gene responsible for FCMD, but these mice did not develop muscular dystrophy, which hindered exploring therapeutic strategies. We hypothesized that dysferlin functions may contribute to muscle cell viability in the knock-in mice; however, pathological interactions between glycosylation abnormalities and dysferlin defects remain unexplored. To investigate contributions of dysferlin deficiency to the pathology of dystroglycanopathy, we have crossed dysferlin-deficient *dysferlin$^{sjl/sjl}$* mice to the fukutin-knock-in *fukutin$^{Hp/-}$* and Large-deficient *Large$^{myd/myd}$* mice, which are phenotypically distinct models of dystroglycanopathy. The *fukutin$^{Hp/-}$* mice do not show a dystrophic phenotype; however, (*dysferlin$^{sjl/sjl}$*: *fukutin$^{Hp/-}$*) mice showed a deteriorated phenotype compared with (*dysferlin$^{sjl/sjl}$*: *fukutin$^{Hp/+}$*) mice. These data indicate that the absence of functional dysferlin in the asymptomatic *fukutin$^{Hp/-}$* mice triggers disease manifestation and aggravates the dystrophic phenotype. A series of pathological analyses using double mutant mice for Large and dysferlin indicate that the protective effects of dysferlin appear diminished when the dystrophic pathology is severe and also may depend on the amount of dysferlin proteins. Together, our results show that dysferlin exerts protective effects on the *fukutin$^{Hp/-}$* FCMD mouse model, and the (*dysferlin$^{sjl/sjl}$*: *fukutin$^{Hp/-}$*) mice will be useful as a novel model for a recently proposed antisense oligonucleotide therapy for FCMD.

Data Availability: The authors confirm that all data underlying the findings are fully available without restriction. All relevant data are within the paper.

Competing Interests: The authors have declared that no competing interests exist.

* Email: toda@med.kobe-u.ac.jp

¶ These authors are joint first authors on this work.

Introduction

Muscular dystrophies are a heterogeneous group of genetic disorders characterized by the progressive loss of muscle strength and integrity. Several lines of evidence have established that the structural linkage between the muscle extracellular matrix and the cytoskeleton is essential in preventing the progression of muscular dystrophy [1]. The dystrophin-glycoprotein complex (DGC) forms the structural linkage, and mutations in components of this complex cause several forms of muscular dystrophy, including Duchenne and limb-girdle muscular dystrophies (LGMDs) [2]. Within the DGC, α- and β-dystroglycans (DG) act as a molecular bridge between the extracellular matrix and the cytoskeleton. α-DG is a highly glycosylated extracellular subunit that functions as a receptor for extracellular matrix proteins such as laminins. O-mannosyl glycosylation and a novel phosphodiester-linked modification of O-mannose, termed post-phosphoryl modification, are necessary for α-DG to serve as a functional laminin receptor [3,4]. α-DG is anchored on the plasma membrane through non-covalent interaction with a transmembrane-type β-DG, which in turn binds to the dystrophin-actin cytoskeleton.

Fukuyama congenital muscular dystrophy (FCMD: MIM 253800) is an autosomal recessive disorder characterized by severe

– 84 –

muscular dystrophy, abnormal neuronal migration associated with mental retardation and, frequently, eye abnormalities [5]. We identified *fukutin*, the gene responsible for FCMD, and a 3-kb SINE-VNTR-*Alu* (SVA) retrotransposon insertion into the 3' UTR of *fukutin* as the founder mutation in FCMD [6]. This insertion causes abnormal splicing that leads to the production of non-functional fukutin protein [7]. The introduction of antisense oligonucleotides that target the splice acceptor and splicing enhancers prevented the pathogenic abnormal splicing by SVA in the cells of FCMD patients as well as model mice that carry the retrotransposal insertion [7]. Point mutations in *fukutin* have been reported in patients both inside and outside Japan, and recent studies have revealed a broad clinical spectrum for fukutin-deficient muscular dystrophies [8]. In FCMD, α-DG is abnormally glycosylated, and its laminin-binding activity is decreased [3]. Several other forms of muscular dystrophy are caused by abnormal glycosylation of α-DG; collectively, these conditions are termed "dystroglycanopathies". More than 10 genes have been identified as causative genes in dystroglycanopathies [9–14], some of which encode products that possess enzyme activities involved in synthesizing O-mannosyl sugar chains on α-DG [15–18]. Fukutin, LARGE, and Fukutin-related protein (FKRP) participate in forming the post-phosphoryl moiety [4,19]. Overall, dystroglycanopathy gene products appear to be involved in O-mannosyl chain synthesis and post-phosphoryl modification; mutations in these pathways commonly result in abnormal glycosylation of α-DG and reduced ligand-binding activity, disrupting the DG-mediated linkage between the extracellular matrix and the cytoskeleton [2].

Defects in DGC components or α-DG glycosylation disrupt the linkage between the extracellular matrix and the cytoskeleton, thus rendering the sarcolemma more susceptible to contraction-induced damage. This is thought to trigger an increase in intracellular Ca^{2+} concentration, eventually leading to necrosis and myofiber degeneration. Myofibers possess an intrinsic mechanism for repair of damaged membranes, and dysferlin plays a pivotal role in the skeletal muscle membrane repair pathway. In humans, dysferlin deficiency leads to LGMD2B, Miyoshi myopathy or a distal myopathy with anterior tibial onset [20]. Dysferlin-deficient mice show defective membrane repair and also develop muscular dystrophy [21]. Several proteins are known to interact with dysferlin [20], and it is expected that these proteins also participate in membrane repair. For example, mitsugumin 53 (MG53, also known as TRIM72) has been implicated in vesicle trafficking to the damage site during the membrane repair process [22].

We previously described a new FCMD mouse model that carries the retrotransposal insertion in the mouse *fukutin* ortholog [23]. These knock-in mice exhibit hypoglycosylated α-DG but do not develop muscular dystrophy. Therefore, these mice are not suitable for testing effectiveness of the antisense oligonucleotide therapy for FCMD. Although skeletal muscle-selective fukutin conditional knock-out mice, namely MCK-fukutin-cKO and Myf5-fukutin-cKO, show dystrophic phenotype [24], they are not applicable for the examination of the antisense oligonucleotide therapy because they do not possess the retrotransposal insertion. We previously reported that the small amount of normally glycosylated α-DG remaining in the skeletal muscle of the knock-in mice prevents muscular dystrophy [23]. However, it is not clear whether this residual glycosylation alone is sufficient to maintain skeletal muscle membrane integrity. We hypothesized that dysferlin functions compensate for presumed membrane fragility caused by a reduced interaction between α-DG and laminin. Furthermore, the exact contribution of dysferlin and

dysferlin-interacting proteins to the pathology of dystroglycanopathy is not known. To investigate this question, we crossed dysferlin-deficient mice with two distinct dystroglycanopathy mouse models and analyzed the resultant phenotypes. In addition, if the double mutant mice carrying the retrotransposal insertion show worse dystrophic phenotype than those of dysferlin mutant mice, they can be the first model for the novel antisense oligonucleotide therapy for FCMD.

Materials and Methods

Animals

Dysferlin-deficient SJL/J mice, a strain with a large deletion in the *Dysf* gene [25], were purchased from Charles River Japan. The transgenic mouse carrying a neo cassette disruption of one *fukutin* allele (*fukutin*$^{+/-}$) [26] and the transgenic knock-in homozygous mutant mouse carrying the retrotransposal insertion in the mouse *fukutin* ortholog (*fukutin*$^{Hp/Hp}$) have been described previously [23]. Genotyping for the *Dysf* mutant allele and the *fukutin* mutant allele was performed as described previously [23,25]. All animal procedures were approved by the Animal Care and Use Committee of Kobe University Graduate School of Medicine (P120202-R2) in accordance with guidelines of Ministry of Education, Culture, Sports, Science and Technology (MEXT) and Japan Society for the Promotion of Science (JSPS). The animals were housed in cages (2–4 mice per cage) with wood-chip bedding in an environmentally controlled room (25°C, 12 h light-dark cycle) and provided food and water *ad libitum* at the animal facility of Kobe University Graduate School of Medicine. Well-trained and skilled researchers and experimental technicians, who have knowledge of methods to prevent unnecessary excessive pain, handled the animals and carried out the experiments. Euthanization was done by cervical dislocation. At sacrifice, the muscles were harvested and snap-frozen in liquid nitrogen (for biochemistry) or in liquid-nitrogen-cooled isopentane (for immunofluorescence and histology). The number and ages of animals used in each experiment is indicated in Figure legends and graphs.

To generate double mutant mice for dysferlin and fukutin deficiency, we crossed dysferlin-deficient SJL/J mice [25] (*dysferlin*$^{sjl/sjl}$; SJL background) with two different lines of *fukutin* mutant mice. One is a transgenic mouse carrying a neo cassette disruption for a single *fukutin* allele (*fukutin*$^{+/-}$; 129-C57BL/6 background) [26] (Fig. 1A, line A). The other is a transgenic knock-in homozygous mutant mouse carrying the retrotransposal insertion in the mouse *fukutin* ortholog [23] (*fukutin*$^{Hp/Hp}$; 129-C57BL/6 background) (Fig. 1A, line B). Heterozygous F1 mice in both lines were intercrossed to obtain the following four genotypes (F2): (*dysferlin*$^{sjl/sjl}$: *fukutin*$^{+/-}$); (*dysferlin*$^{sjl/+}$: *fukutin*$^{+/-}$); (*dysferlin*$^{sjl/+}$: *fukutin*$^{Hp/Hp}$); and (*dysferlin*$^{sjl/sjl}$: *fukutin*$^{Hp/Hp}$). We further crossed (*dysferlin*$^{sjl/sjl}$: *fukutin*$^{+/-}$) with (*dysferlin*$^{sjl/+}$: *fukutin*$^{Hp/Hp}$) mice or (*dysferlin*$^{sjl/+}$: *fukutin*$^{+/-}$) with (*dysferlin*$^{sjl/sjl}$: *fukutin*$^{Hp/Hp}$) mice (Fig. 1A, highlighted with gray) to produce four genotypes (F3): (*dysferlin*$^{sjl/+}$: *fukutin*$^{Hp/+}$); (*dysferlin*$^{sjl/+}$: *fukutin*$^{Hp/-}$); (*dysferlin*$^{sjl/sjl}$: *fukutin*$^{Hp/+}$); and (*dysferlin*$^{sjl/sjl}$: *fukutin*$^{Hp/-}$). To generate double mutant mice for dysferlin and Large deficiency, we crossed dysferlin-deficient SJL/J mice (C57BL/6 backcross 7) with Large-deficient *Large*^{myd} mice (*Large*$^{myd/myd}$; C57BL/6 background) [27,28]. Heterozygous F1 mice were intercrossed and the following four genotypes were used for the analyses (F2): (*dysferlin*$^{sjl/+}$: *Large*$^{myd/+}$); (*dysferlin*$^{sjl/sjl}$: *Large*$^{myd/+}$); (*dysferlin*$^{sjl/+}$: *Large*$^{myd/myd}$); and (*dysferlin*$^{sjl/sjl}$: *Large*$^{myd/myd}$). For more effective breeding, we crossed (*dysferlin*$^{sjl/+}$: *Large*$^{myd/+}$) mice with (*dysferlin*$^{sjl/sjl}$: *Large*$^{myd/+}$) mice (Fig. 1B). (*Dysferlin*$^{+/+}$: *Large*$^{myd/myd}$) mice were obtained from
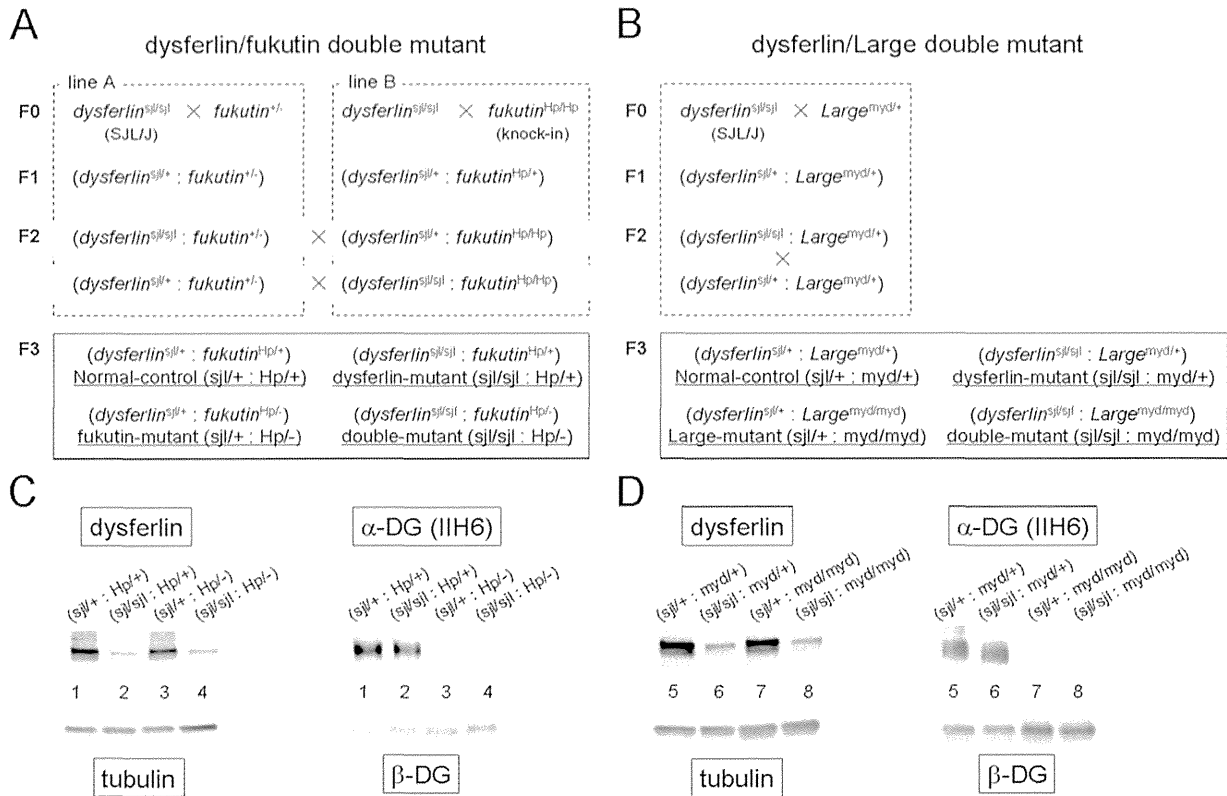
Figure 1. Generation of double-mutant mice exhibiting both abnormal α-DG glycosylation and reduced dysferlin expression. (A, B) Breeding strategy for the generation of double-mutant mice. sjl represents the *dysferlin* mutant allele, myd represents the *Large* mutant allele, and Hp represents the transgenic allele carrying the retrotransposal insertion in *fukutin*. Hp/+ represents a carrier with the insertion in *fukutin*. Hp/− represents a compound heterozygote carrying the insertion and a neo-disrupted allele. For the dysferlin/fukutin double mutant line, we used mice carrying *dysferlin*$^{sjl/+}$ and *fukutin*$^{Hp/+}$ as the normal control (*dysferlin*$^{sjl/+}$: *fukutin*$^{Hp/+}$); *dysferlin*$^{sjl/sjl}$ and *fukutin*$^{Hp/+}$ as the *dysferlin*-mutant (*dysferlin*$^{sjl/sjl}$: *fukutin*$^{Hp/+}$); *dysferlin*$^{sjl/+}$ and *fukutin*$^{Hp/−}$ as the *fukutin*-mutant (*dysferlin*$^{sjl/+}$: *fukutin*$^{Hp/−}$); and *dysferlin*$^{sjl/sjl}$ and *fukutin*$^{Hp/−}$ as the double-mutant (*dysferlin*$^{sjl/sjl}$: *fukutin*$^{Hp/−}$). For the dysferlin/Large double mutant line, we used mice carrying *dysferlin*$^{sjl/+}$ and *Large*$^{myd/+}$ as the normal control (*dysferlin*$^{sjl/+}$: *Large*$^{myd/+}$); *dysferlin*$^{sjl/sjl}$ and *Large*$^{myd/+}$ as the *dysferlin*-mutant (*dysferlin*$^{sjl/sjl}$: *Large*$^{myd/+}$); *dysferlin*$^{sjl/+}$ and *Large*$^{myd/myd}$ as the *Large*-mutant (*dysferlin*$^{sjl/+}$: *Large*$^{myd/myd}$); and *dysferlin*$^{sjl/sjl}$ and *Large*$^{myd/myd}$ as the double mutant (*dysferlin*$^{sjl/sjl}$: *Large*$^{myd/myd}$). (C, D) Abnormal α-DG glycosylation and reduced dysferlin protein expression. Solubilized skeletal muscle samples from each genotype were subjected to Western blot analysis for dysferlin protein expression (left panel). Tubulin was used as a loading control. The solubilized fractions were further enriched for DG by WGA-beads, and the DG-enriched fractions were subjected to Western blotting with the monoclonal IIH6 antibody, which recognizes glycosylated α-DG (right panel). β-DG was used as a loading control. The (*dysferlin*$^{sjl/+}$: *fukutin*$^{Hp/+}$), (*dysferlin*$^{sjl/sjl}$: *fukutin*$^{Hp/+}$), (*dysferlin*$^{sjl/+}$: *fukutin*$^{Hp/−}$), and (*dysferlin*$^{sjl/sjl}$: *fukutin*$^{Hp/−}$) mice are abbreviated as (sjl/+: Hp/+), (sjl/sjl: Hp/+), (sjl/+: Hp/−), and (sjl/sjl: Hp/−), respectively. The (*dysferlin*$^{sjl/+}$: *Large*$^{myd/+}$), (*dysferlin*$^{sjl/sjl}$: *Large*$^{myd/+}$), (*dysferlin*$^{sjl/+}$: *Large*$^{myd/myd}$), and (*dysferlin*$^{sjl/sjl}$: *Large*$^{myd/myd}$) mice are abbreviated as (sjl/+: myd/+), (sjl/sjl: myd/+), (sjl/+: myd/myd), and (sjl/sjl: myd/myd), respectively.
doi:10.1371/journal.pone.0106721.g001

the dysferlin/Large double mutant line and *Large*^{myd} mouse colonies.

Antibodies

Antibodies used in Western blotting and immunofluorescence were as follows: mouse monoclonal antibody 8D5 against β-DG (Novocastra); mouse monoclonal antibody IIH6 against α-DG (Millipore); affinity-purified goat polyclonal antibody against the α-DG core protein (AP-074G-C) [23]; mouse monoclonal antibody NCL-Hamlet against dysferlin (Novocastra); rat monoclonal antibody against mouse F4/80 (BioLegend); rabbit polyclonal antibody against collagen I (AbD serotec); rabbit polyclonal antibody against albumin (DAKO); mouse monoclonal antibody against caveolin-3 (BD Transduction Laboratories); rabbit polyclonal antibody against caveolin-3 (Abcam); and rabbit polyclonal antibody against Trim72 (MG53) (Abcam).

Protein preparation and Western blotting

DG was enriched from solubilized skeletal muscle as described previously [23]. Briefly, skeletal muscles were solubilized in Tris-buffered saline (TBS) containing 1% Triton X-100 and protease inhibitors (Nacalai). The solubilized fraction was incubated with wheat germ agglutinin (WGA)-agarose beads (Vector Laboratories) at 4°C for 16 h, and then DG was eluted with SDS-PAGE loading buffer. For detection of dysferlin and dysferlin-interacting proteins, RIPA buffer (1% NP-40, 0.5% DOC, and 0.1% SDS in TBS with protease inhibitors) was used for protein extraction from skeletal muscle. For this experiment, we used *fukutin*$^{Hp/−}$ mice and litter control *fukutin*$^{Hp/+}$ mice that were backcrossed to C57BL/6 mice more than 10 times. Protein concentration of the solubilized fractions was measured by Lowry methods, using BSA as a standard. Proteins were separated using 3–15% linear gradient SDS-gels. Gels were transferred to polyvinylidene fluoride

− 86 −

(PVDF) membrane (Millipore). Blots were probed with antibodies and then developed with horseradish peroxidase (HRP)-enhanced chemiluminescence (Supersignal West Pico, Pierce; or ECL Plus, GE Healthcare). Protein bands were detected using the LAS-4000 system (Fujifilm), and band intensities were quantified using Multi Gauge V3.2 software (Fujifilm). Statistical analysis was performed with a two-tailed unpaired t test. A p value of <0.05 was considered to be significant.

Histological and Immunofluorescence analysis

For H&E staining, cryosections (7 μm) were stained for 2 min in hematoxylin, 1 min in eosin, and then dehydrated with ethanol and xylenes. For Masson trichrome staining, sections were fixed with Bouin's solution (Sigma) for 1 hour at 60°C. The slides were incubated in solution A (5% trichloroacetic acid, 5% potassium dichromate) for 30 min, and then stained with Weigert's iron hematoxylin (Muto Chemical Co Ltd) for 15 min. After a rinse with 0.5% HCl in 70% ethanol and a subsequent rinse with warm water, the slides were incubated in solution B (0.5% phospho-tungstic acid, 2.5% phosphomolybdic acid) for 1 min, and then stained with FUCHSIN-PONCEAU solution. The slides were washed with 1% acetic acid, incubated in 2.5% phosphomolybdic acid for 5 min, washed with 1% acetic acid, stained with aniline blue, washed with 1% acetic acid, dehydrated, and mounted.

For immunofluorescence analysis, sections were treated with cold ethanol/acetone (1:1) for 1 min, blocked with 5% goat serum in MOM Mouse Ig Blocking Reagent (Vector Laboratories) at room temperature for 1 h, and then incubated with primary antibodies diluted in MOM Diluent (Vector Laboratories) overnight at 4°C. The slides were washed with PBS and incubated with Alexa Fluor 488-conjugated or Alexa Fluor 555-conjugated secondary antibodies (Molecular Probes) at room temperature for 30 min. Permount (Fisher Scientific) and TISSU MOUNT (Shiraimatsu Kikai) were used for H&E staining and immunofluorescence, respectively. Sections were observed under fluorescence microscopy (Leica DMR, Leica Microsystems).

For quantitative evaluation of muscle pathology, the percentages of myofiber with centrally located nuclei were counted for at least 1,000 fibers for each genotype (n>4). For evaluation of the F4/80-positive and the collagen I-positive area, the immunofluorescence signal was quantitatively measured using Image J software. Statistical analysis was performed using values represent means with standard deviations, and p values <0.05 were considered significant (Student's t-test and Mann–Whitney U test).

Results

Generation of double mutant mice exhibiting both abnormal glycosylation of α-DG and dysferlin deficiency

To generate double mutant mice, we crossed dysferlin-deficient SJL/L mice ($dysferlin^{sjl/sjl}$) [25] with two distinct dystroglycano-pathy models, fukutin-deficient or Large-deficient mice. Previously we reported a transgenic knock-in homozygous mutant mouse carrying the retrotransposal insertion in the mouse fukutin ortholog ($fukutin^{Hp/Hp}$) [23]. Compound heterozygous mice carrying the retrotransposal insertion and a neo cassette fukutin disruption ($fukutin^{Hp/-}$) showed more abnormal glycosylation of α-DG than did mice homozygous for the insertion ($fukutin^{Hp/Hp}$ mice), although $fukutin^{Hp/-}$ mice did show a detectable amount of residual α-DG glycosylation [23]. For the current study, we generated double mutant mice with the ($dysferlin^{sjl/sjl}$: $fukutin^{Hp/-}$) genotype (Fig. 1A). The other dystroglycanopathy model, Large-deficient $Large^{myd}$ mouse ($Large^{myd/myd}$) [27,28] show abnormal glycosylation with no detectable amount of properly glycosylated α-DG. The ligand binding activity of α-DG in $Large^{myd/myd}$ mice is greatly reduced compared with that in $fukutin^{Hp/-}$ mice [23]. Breeding strategies, genotypes, and abbreviations for these double mutant mice and their controls are shown in Figure 1A and 1B.

To confirm reduced protein expression of dysferlin and abnormal glycosylation of α-DG in these mice, we prepared solubilized fractions from skeletal muscle extracts and enriched for α-DG using wheat germ agglutinin (WGA)-agarose beads. Western blot analysis showed a dramatic reduction of dysferlin protein in skeletal muscle from ($dysferlin^{sjl/sjl}$: $fukutin^{Hp/+}$), ($dysferlin^{sjl/sjl}$: $fukutin^{Hp/-}$), ($dysferlin^{sjl/sjl}$: $Large^{myd/+}$), and ($dysferlin^{sjl/sjl}$: $Large^{myd/myd}$) mice (Fig. 1C and D). We also confirmed a significant reduction of reactivity against the monoclonal antibody IIH6, which recognizes glycosylated epitopes on α-DG that are necessary for laminin binding activity, in ($dysferlin^{sjl/+}$: $fukutin^{Hp/-}$), ($dysferlin^{sjl/sjl}$: $fukutin^{Hp/-}$), ($dysferlin^{sjl/+}$: $Large^{myd/myd}$), and ($dysferlin^{sjl/sjl}$: $Large^{myd/myd}$) (Fig. 1C and D). Overall, these data confirmed the production of model mice with four biochemically distinct genotypes in each double mutant line.

More severe muscular dystrophy in ($dysferlin^{sjl/sjl}$: $fukutin^{Hp/-}$) than in ($dysferlin^{sjl/sjl}$: $fukutin^{Hp/+}$) mice

We examined the histopathology of ($dysferlin^{sjl/sjl}$: $fukutin^{Hp/-}$) mice by hematoxylin and eosin (H&E) staining. The ($dysferlin^{sjl/+}$: $fukutin^{Hp/-}$) mice showed no obvious pathological features of muscular dystrophy (Fig. 2). The ($dysferlin^{sjl/sjl}$: $fukutin^{Hp/+}$) mice showed mild dystrophic changes such as the presence of necrotic fibers and centrally located nuclei (Fig. 2). The phenotypes of ($dysferlin^{sjl/+}$: $fukutin^{Hp/-}$) and ($dysferlin^{sjl/sjl}$: $fukutin^{Hp/+}$) mice are similar to those described previously for retrotransposon knock-in fukutin mutant mice and dysferlin-deficient SJL/J mice, respectively [23,25]. These results also indicate that disruption of one dysferlin or one fukutin allele does not affect the phenotype of $fukutin^{Hp/-}$ or $dysferlin^{sjl/sjl}$ single mutant mice, respectively. H&E staining showed that the ($dysferlin^{sjl/sjl}$: $fukutin^{Hp/-}$) mice showed further progressed and more severe dystrophic features than did the ($dysferlin^{sjl/sjl}$: $fukutin^{Hp/+}$) mice in quadriceps (Quad), gastrocnemius (Gast), and tibialis anterior (TA) muscles (Fig. 2A and Fig. 3A). Comparison of the percentage of muscle fibers with centrally located nuclei confirmed a more severe dystrophic phenotype in the ($dysferlin^{sjl/sjl}$: $fukutin^{Hp/-}$) mice than that in the ($dysferlin^{sjl/sjl}$: $fukutin^{Hp/+}$) mice (Fig. 2B).

To compare the pathological severity in ($dysferlin^{sjl/sjl}$: $fukutin^{Hp/-}$) and ($dysferlin^{sjl/sjl}$: $fukutin^{Hp/+}$) skeletal muscle more precisely, we counted the percentage of muscle fibers (TA) with centrally located nuclei at different ages (Fig. 3A and B). In 8-week-old mice, we observed a few fibers with centrally located nuclei and necrotic fibers in both the ($dysferlin^{sjl/sjl}$: $fukutin^{Hp/+}$) and the ($dysferlin^{sjl/sjl}$: $fukutin^{Hp/-}$) mice, but no significant differences were seen between the two (data not shown). At 15 weeks and 30 weeks of age, the ($dysferlin^{sjl/sjl}$: $fukutin^{Hp/-}$) mice show significantly more fibers with centrally located nuclei than do the ($dysferlin^{sjl/sjl}$: $fukutin^{Hp/+}$) mice (Fig. 3B). The proportion of fibers with centrally located nuclei in the ($dysferlin^{sjl/sjl}$: $fukutin^{Hp/-}$) mice increased with age. These results indicate more frequent cycles of muscle cell degeneration and regeneration in the ($dysferlin^{sjl/sjl}$: $fukutin^{Hp/-}$) mice. We next compared infiltration of macrophage and connective tissue as indicators of disease severity. Immunofluorescence analysis using the monoclonal F4/80 antibody, a marker for macrophages, indicated that macrophage infiltration was increased in ($dysferlin^{sjl/sjl}$: $fukutin^{Hp/-}$) skeletal muscle compared with ($dysferlin^{sjl/sjl}$: $fukutin^{Hp/+}$) skeletal
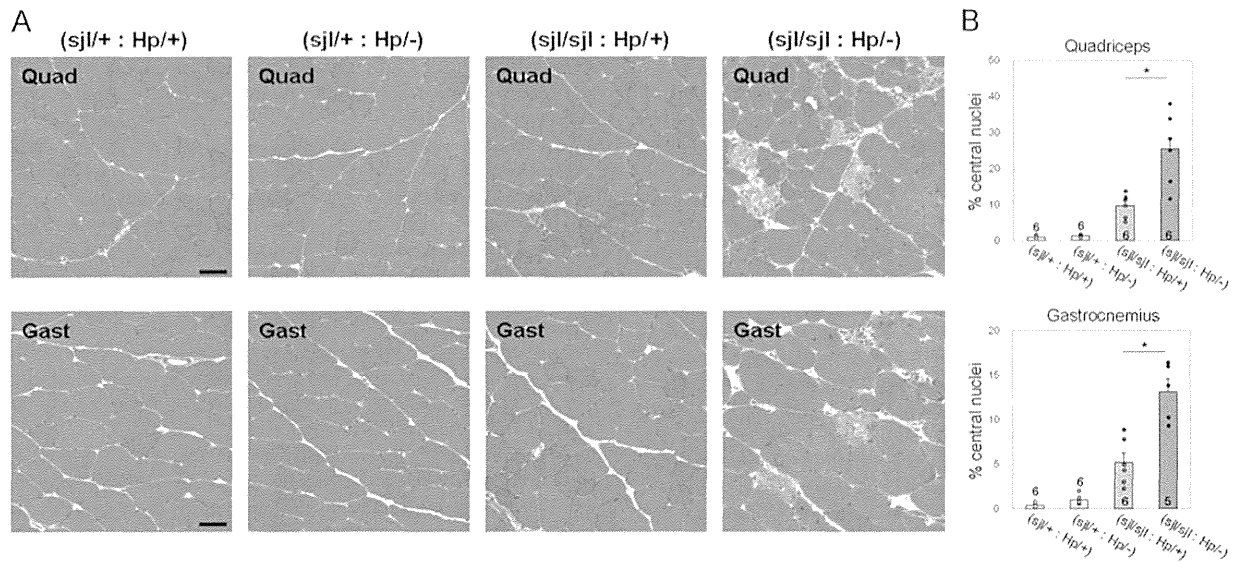
Figure 2. Histological analysis of skeletal muscle from dysferlin/fukutin double mutant mice. (A) Quadriceps (Quad) and gastrocnemius (Gast) muscle tissues from the four mouse genotypes at 15 weeks were analyzed by H&E staining. Bar, 50 μm. (B) Myofibers with centrally located nuclei were counted and quantitatively compared between ($dysferlin^{sjl/sjl}$: $fukutin^{Hp/+}$) and ($dysferlin^{sjl/sjl}$: $fukutin^{Hp/-}$) mice (*, $p<0.05$). Data shown are mean ± s.e.m. for each group (n is indicated in the graph). The ($dysferlin^{sjl/+}$: $fukutin^{Hp/+}$), ($dysferlin^{sjl/+}$: $fukutin^{Hp/-}$), ($dysferlin^{sjl/sjl}$: $fukutin^{Hp/+}$), and ($dysferlin^{sjl/sjl}$: $fukutin^{Hp/-}$) mice are abbreviated as (sjl/+: Hp/+), (sjl/+: Hp/−), (sjl/sjl: Hp/+), and (sjl/sjl: Hp/−), respectively.

doi:10.1371/journal.pone.0106721.g002

muscle (Fig. 4A). Quantification of F4/80-immunofluorescence signals confirmed significant increases of macrophage infiltration in ($dysferlin^{sjl/sjl}$: $fukutin^{Hp/-}$) skeletal muscle (Fig. 4B). Masson trichrome staining revealed that the fibrotic area was increased in ($dysferlin^{sjl/sjl}$: $fukutin^{Hp/-}$) skeletal muscle (Fig. 4C). Quantification of immunofluorescence signals for collagen I further supported significant increases of connective tissue infiltrations in ($dysferlin^{sjl/sjl}$: $fukutin^{Hp/-}$) skeletal muscles (Fig. 4D). These data are indicative of further progressed and more severe dystrophic phenotypes in ($dysferlin^{sjl/sjl}$: $fukutin^{Hp/-}$) skeletal muscle. Importantly, although the ($dysferlin^{sjl/+}$: $fukutin^{Hp/-}$) mice do not show muscle pathology, the ($dysferlin^{sjl/sjl}$: $fukutin^{Hp/-}$) mice show a more severe phenotype than do the ($dysferlin^{sjl/sjl}$: $fukutin^{Hp/+}$) mice, suggesting that dysferlin plays a protective role in preventing disease manifestation in the ($dysferlin^{sjl/+}$: $fukutin^{Hp/-}$) mice.

Our previous data and those of others suggest that muscle cell membrane fragility due to loss of DG or its functional glycosylation triggers disease manifestation [24,29]. However, we have not observed evidence indicating membrane fragility in $fukutin^{Hp/-}$ skeletal muscle [23]. To investigate whether membrane fragility is associated mechanistically with the deteriorated phenotype of the ($dysferlin^{sjl/sjl}$: $fukutin^{Hp/-}$) mice, we analyzed the population of albumin-positive muscle fibers. Intracellular albumin staining often is used as an indicator of muscle fiber damage or increased membrane permeability [30]. Immunofluorescence analysis suggested that the albumin-positive myofibers were almost absent in both ($dysferlin^{sjl/+}$: $fukutin^{Hp/+}$) and ($dysferlin^{sjl/+}$: $fukutin^{Hp/-}$) and only sparsely observed in ($dysferlin^{sjl/sjl}$: $fukutin^{Hp/+}$) skeletal muscles, whereas they appeared increased in ($dysferlin^{sjl/sjl}$: $fukutin^{Hp/-}$) skeletal muscle (Fig. 5A). Quantification of albumin-positive fibers also confirmed significant deterioration of the myofiber membrane fragility in the ($dysferlin^{sjl/sjl}$: $fukutin^{Hp/-}$) mice (Fig. 5B). These data suggest that skeletal muscle fibers in ($dysferlin^{sjl/+}$: $fukutin^{Hp/-}$) mice have latent membrane fragility, which is protected partially by dysferlin

functions, and membrane fragility caused by synergy of reduced α-DG glycosylation and dysferlin-deficiency underlies the deteriorated phenotype of the ($dysferlin^{sjl/sjl}$: $fukutin^{Hp/-}$) mice.

We examined whether dysferlin itself and/or its interacting proteins, caveolin-3 [31] and MG53 [22], are compensatory upregulated in $fukutin^{Hp/-}$ mice. Western blot analysis showed that levels of dysferlin, caveolin-3, and MG53 were not significantly different between $fukutin^{Hp/-}$ and $fukutin^{Hp/+}$ skeletal muscle (Fig. S1A and B). Immunofluorescence analysis also showed no obvious change in dysferlin expression pattern between $fukutin^{Hp/-}$ and $fukutin^{Hp/+}$ skeletal muscle (Fig. S1C).

Characterization of muscular dystrophic changes in ($dysferlin^{sjl/sjl}$: $Large^{myd/myd}$) mice

We subsequently analyzed the histopathology of ($dysferlin^{sjl/sjl}$: $Large^{myd/myd}$) mice. $Large^{myd/myd}$ mice show severe muscular dystrophic phenotypes such as infiltration of connective and fat tissues and marked variation in fiber size [28]. Almost all α-DG is hypoglycosylated in $Large^{myd/myd}$ mice [23]. We confirmed that the pathology of ($dysferlin^{sjl/+}$: $Large^{myd/myd}$) mice was more severe than that in ($dysferlin^{sjl/sjl}$: $Large^{myd/+}$) mice (Fig. 6). To examine whether the dysferlin functions have protective roles in $Large^{myd/myd}$ skeletal muscle, we compared the pathology in ($dysferlin^{sjl/+}$: $Large^{myd/myd}$) and ($dysferlin^{sjl/sjl}$: $Large^{myd/myd}$) mice. The ($dysferlin^{sjl/+}$: $Large^{myd/myd}$) mice showed necrotic and centrally nucleated fibers, indicating frequent cycles of muscle degeneration and regeneration (Fig. 6C). In addition, some animals showed signs of advanced muscular dystrophic changes such as variations in fiber size and connective tissue infiltration (Fig. 6D). The ($dysferlin^{sjl/sjl}$: $Large^{myd/myd}$) mice exhibited severe pathology, including marked variation in fiber size and large areas with infiltration (Fig. 6E and F). We evaluated these pathologies quantitatively by measuring the areas of macrophage or connective tissue infiltration and the population of albumin-positive
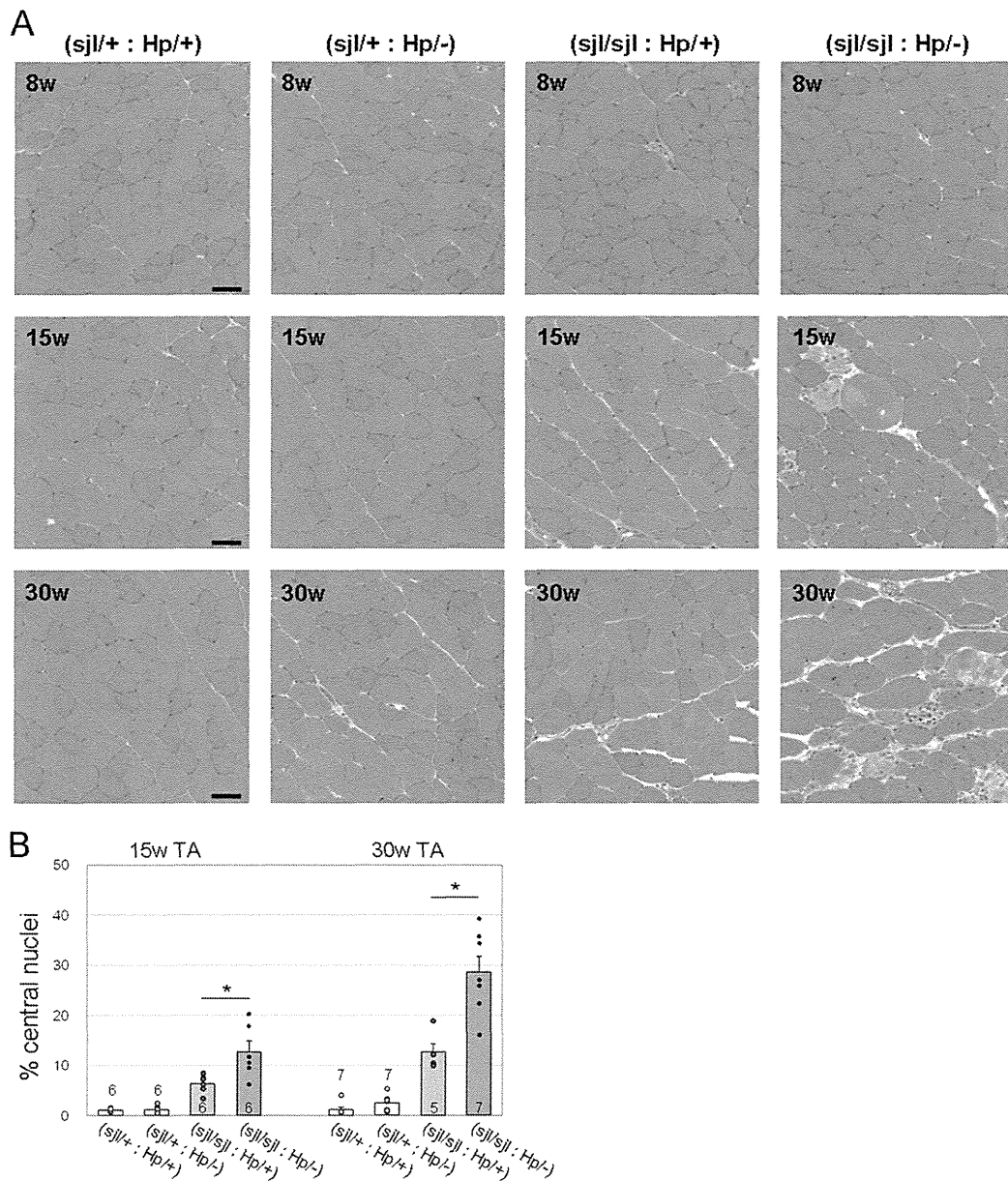
− 88 −

Figure 3. Pathological comparisons between (dysferlin$^{sjl/sjl}$: fukutin$^{Hp/+}$) and (dysferlin$^{sjl/sjl}$ and fukutin$^{Hp/-}$) mice. (A) H&E staining of TA muscle from (dysferlin$^{sjl/+}$: fukutin$^{Hp/+}$), (dysferlin$^{sjl/+}$: fukutin$^{Hp/-}$), (dysferlin$^{sjl/sjl}$: fukutin$^{Hp/+}$) and (dysferlin$^{sjl/sjl}$: fukutin$^{Hp/-}$) mice at 8, 15 and 30 weeks. Bar, 50 μm. (B) Myofibers with centrally located nuclei were counted and quantitatively compared between (dysferlin$^{sjl/sjl}$: fukutin$^{Hp/+}$) and (dysferlin$^{sjl/sjl}$: fukutin$^{Hp/-}$) mice at 15 and 30 weeks (*, $p < 0.05$). Data shown are mean ± s.e.m. for each group (n is indicated in the graph). The (dysferlin$^{sjl/+}$: fukutin$^{Hp/+}$), (dysferlin$^{sjl/+}$: fukutin$^{Hp/-}$), (dysferlin$^{sjl/sjl}$: fukutin$^{Hp/+}$), and (dysferlin$^{sjl/sjl}$: fukutin$^{Hp/-}$) mice are abbreviated as (sjl/+: Hp/+), (sjl/+: Hp/−), (sjl/sjl: Hp/+), and (sjl/sjl: Hp/−), respectively.
doi:10.1371/journal.pone.0106721.g003

muscle fibers (Fig. 6I, J, and K). Both the macrophage-infiltrated area and the population of albumin-positive muscle fibers tended to be larger in (dysferlin$^{sjl/sjl}$: Large$^{myd/myd}$) than in (dysferlin$^{sjl/+}$: Large$^{myd/myd}$); however, we did not observe statistically significant differences between the two groups. Furthermore, quantification of collagen I immunofluorescence showed no significant difference in connective tissue infiltration between (dysferlin$^{sjl/sjl}$: Large$^{myd/myd}$) and (dysferlin$^{sjl/+}$: Large$^{myd/myd}$) skeletal muscles. These

results suggest that dysferlin function produces limited protective effects against the progression of severe muscular dystrophy in Large$^{myd/myd}$ mice. Interestingly, however, when compared with the (dysferlin$^{+/+}$: Large$^{myd/myd}$) mice, the (dysferlin$^{sjl/sjl}$: Large$^{myd/myd}$) mice showed significant increases in F4/80, collagen I and intracellular albumin staining (Fig. 6I, J, and K). The amount of dysferlin protein in total lysates from (dysferlin$^{sjl/sjl}$: Large$^{myd/myd}$) and (dysferlin$^{sjl/+}$: Large$^{myd/myd}$) skeletal muscles was estimated to
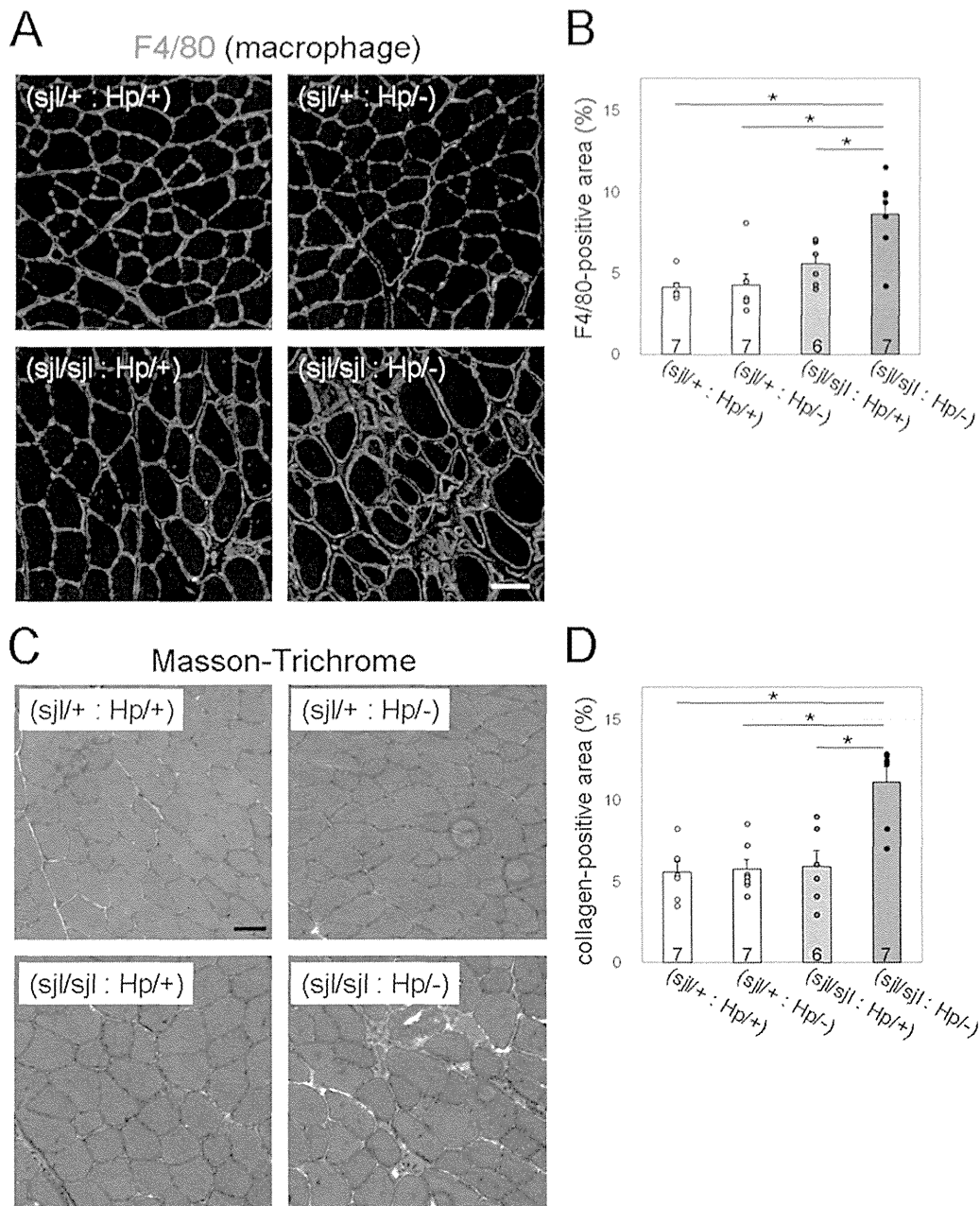
Figure 4. Macrophage and connective tissue infiltration in dysferlin/fukutin double mutant mice. (A) Macrophage infiltration was determined by immunofluorescence analysis using the F4/80 antibody (red). The sarcolemma and nuclei were stained by laminin (green) and DAPI (blue), respectively. TA muscle sections from 30-week-old mice were used. Bar, 50 μm. (B) F4/80-positive immunofluorescence signals were quantified using Image J software. (C) Connective tissue infiltration was determined by Masson-Trichrome staining. TA muscle sections from 30-week-old mice were used. Bar, 50 μm. (D) Quantitative analysis of connective tissue infiltration, determined by immunofluorescence analysis using anti-collagen I antibody. The collagen I-positive area was quantified using Image J software. For quantitative analysis (B and D), data shown are mean ± s.e.m. for each group (n is indicated in the graph; *, $p<0.05$). The (dysferlin$^{sjl/+}$: fukutin$^{Hp/+}$), (dysferlin$^{sjl/+}$: fukutin$^{Hp/-}$), (dysferlin$^{sjl/sjl}$: fukutin$^{Hp/+}$), and (dysferlin$^{sjl/sjl}$: fukutin$^{Hp/-}$) mice are abbreviated as (sjl/+: Hp/+), (sjl/+: Hp/-), (sjl/jl: Hp/+), and (sjl/sjl: Hp/-), respectively.
doi:10.1371/journal.pone.0106721.g004

be ~20% and ~60% of that from (dysferlin$^{+/+}$: Large$^{myd/myd}$) muscle, respectively (Fig. 6L). These results suggest that the dramatic reduction in the amount/activity of dysferlin protein may be associated with a worse phenotype in the (dysferlin$^{sjl/sjl}$:

Large$^{myd/myd}$) mice. Overall, our results suggest that the protective effects of dysferlin on dystroglycanopathy phenotype appear to be diminished when the dystrophic pathology is severe and progressive and also may depend on the amount of dysferlin proteins.
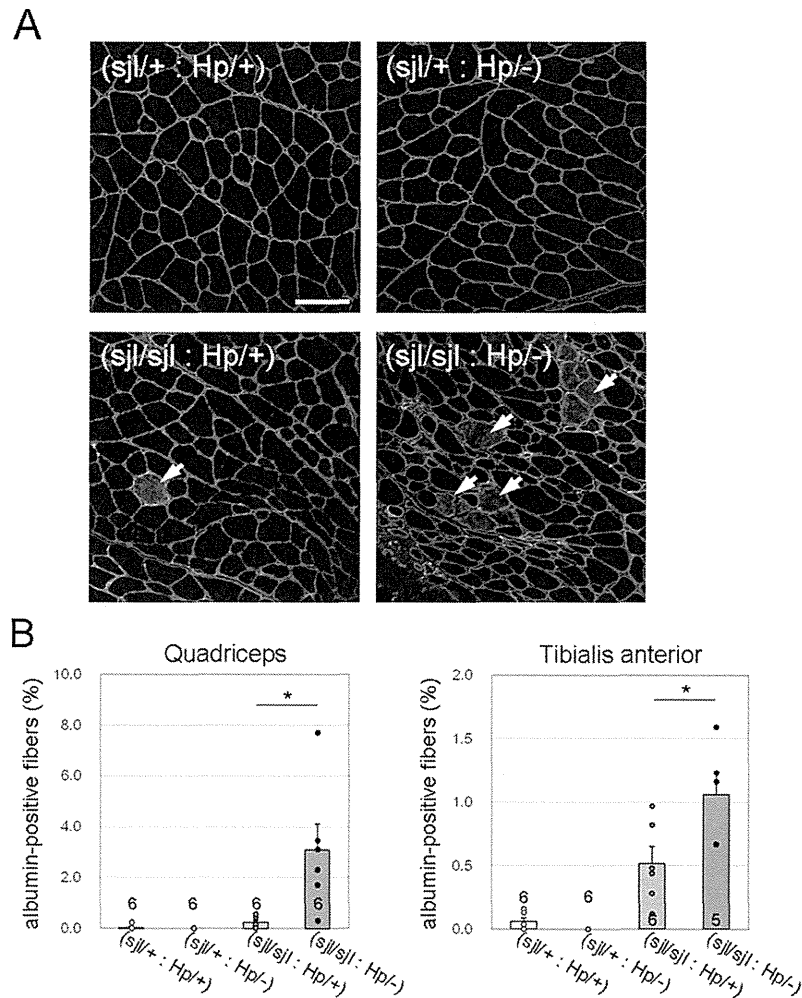
– 90 –

A

B

Figure 5. Myofiber membrane fragility in dysferlin/fukutin double mutant mice. (A) Intracellular albumin was determined by immunofluorescence (red). Myofibers are marked by laminin staining (green). Arrows indicate myofibers with intracellular albumin. Images were taken from quadriceps muscle sections of 15-week-old mice. Bar, 100 μm. (B) Myofibers with intracellular albumin were counted and statistically compared between ($dysferlin^{sjl/sjl}$: $fukutin^{Hp/+}$) and ($dysferlin^{sjl/sjl}$: $fukutin^{Hp/-}$) mice. Quadriceps and TA muscle sections from 15-week-old mice were analyzed. Data shown are mean ± s.e.m. for each group (n is indicated in the graph; *, $p<0.05$). The ($dysferlin^{sjl/+}$: $fukutin^{Hp/+}$), ($dysferlin^{sjl/+}$: $fukutin^{Hp/-}$), ($dysferlin^{sjl/sjl}$: $fukutin^{Hp/+}$), and ($dysferlin^{sjl/sjl}$: $fukutin^{Hp/-}$) mice are abbreviated as (sjl/+: Hp/+), (sjl/+: Hp/−), (sjl/sjl: Hp/+), and (sjl/sjl: Hp/−), respectively.
doi:10.1371/journal.pone.0106721.g005

Discussion

Here we have characterized the contribution of dysferlin-deficiency to the pathology of dystroglycanopathy using double-mutant mice for dysferlin and α-DG glycosylation. To date, several dystroglycanopathy model mice have been established. $Large^{myd}$ mice [28] and knock-in mice carrying the FKRP P448L mutation [32] show no detectable amounts of functionally glycosylated α-DG, no laminin binding activity, and progressive muscular dystrophy. On the other hand, other dystroglycanopathy mouse models do not show a muscular dystrophy phenotype [23]. We previously reported that a small amount of intact α-DG in $fukutin^{Hp/-}$ mice is sufficient to maintain muscle cell integrity, thus preventing muscular dystrophy [23]. These results and others suggest that the presence of functionally glycosylated α-DG can decrease disease severity [33,34]. In the present study, however, we showed that although

($dysferlin^{sjl/+}$: $fukutin^{Hp/-}$) mice did not exhibit a muscular dystrophy phenotype, ($dysferlin^{sjl/sjl}$: $fukutin^{Hp/-}$) mice developed a more exacerbated phenotype than did the $dysferlin$ single-mutant ($dysferlin^{sjl/sjl}$: $fukutin^{Hp/+}$) mice. It has been widely accepted that α-DG glycosylation plays an important role in preventing disease-causing membrane fragility by maintaining a tight association between the basement membrane and the muscle cell membrane, and its defects produce muscle membrane that is susceptible to damage [24,29]. The synergically exacerbated phenotype of the ($dysferlin^{sjl/sjl}$: $fukutin^{Hp/-}$) mice suggests latent membrane fragility in $fukutin$-deficient $fukutin^{Hp/-}$ skeletal muscle. Indeed, the increased number of intracellular albumin-positive fibers in the ($dysferlin^{sjl/sjl}$: $fukutin^{Hp/-}$) mice also supports this hypothesis. It is assumed in the $fukutin^{Hp/-}$ myofiber that interaction between the basement membrane and the cell membrane may be weakened, and therefore disease-causative membrane damage could occur during
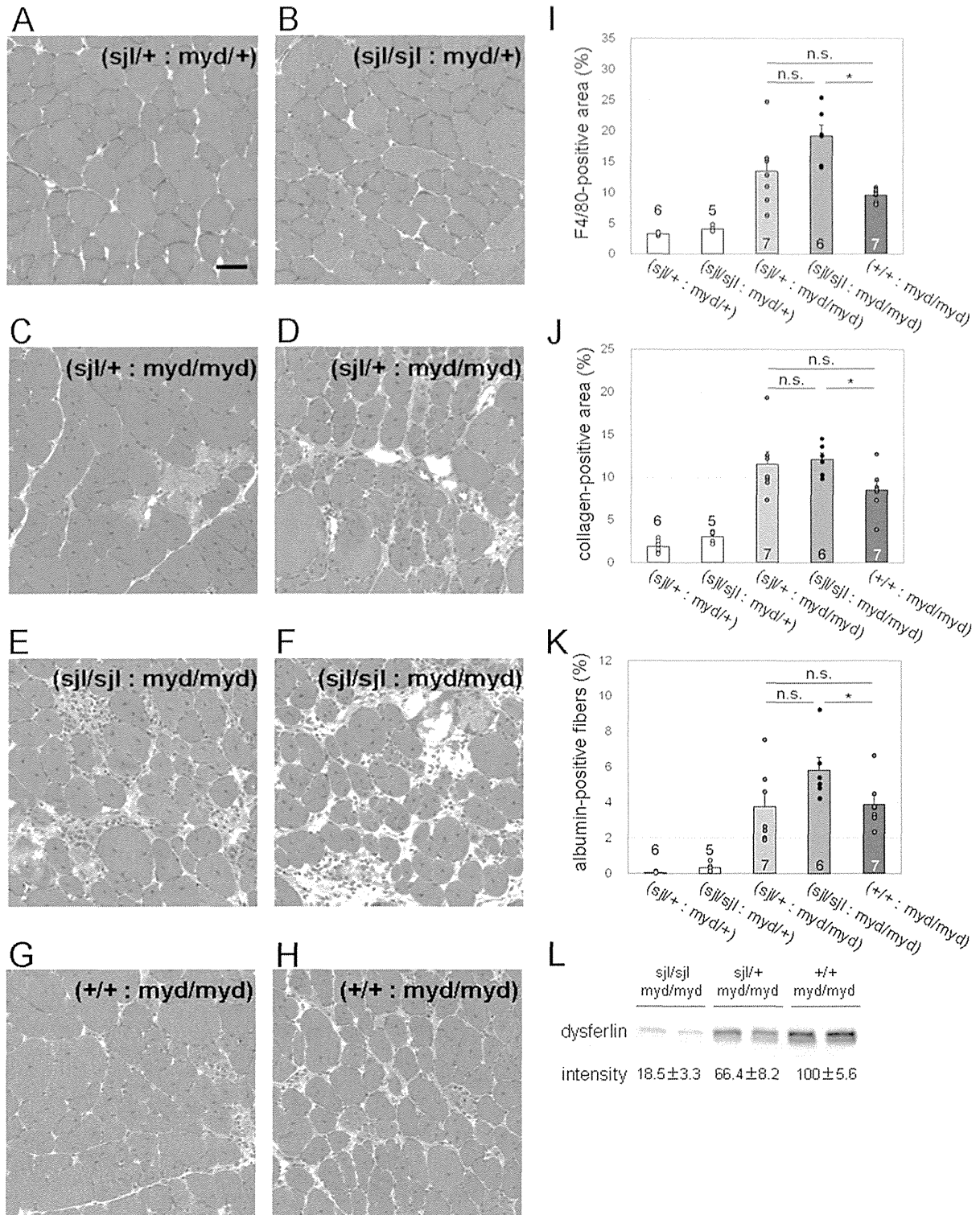
Figure 6. Histopathological analysis of skeletal muscle from dysferlin/Large double mutant mice. (A–H) H&E staining of TA muscle from [(dysferlin$^{sjl/+}$: Large$^{myd/+}$), A], [(dysferlin$^{sjl/sjl}$: Large$^{myd/+}$), B], [(dysferlin$^{sjl/+}$: Large$^{myd/myd}$), C and D], [(dysferlin$^{sjl/sjl}$: Large$^{myd/myd}$), E and F], and [(dysferlin$^{+/}$ $^{+}$: Large$^{myd/myd}$), G and H] mice at 15 weeks. Bar, 50 µm. (I) Quantitative analysis of macrophage infiltration, determined by immunofluorescence analysis using F4/80 antibody. (J) Quantitative analysis of connective tissue infiltration determined by immunofluorescence analysis using

anti-collagen I antibody. (K) Quantitative analysis of the proportion of myofibers containing intracellular albumin. For quantitative analysis (I–K), data shown are mean ± s.e.m. for each group (n is indicated in the graph; *, $p < 0.05$; n.s., not significant). (L) Western blot analysis and quantification of dysferlin expression in the total skeletal muscle lysate from (dysferlin$^{sjl/sjl}$: Large$^{myd/myd}$), (dysferlin$^{sjl/+}$: Large$^{myd/myd}$), and (dysferlin$^{+/+}$: Large$^{myd/myd}$) mice. A representative two individual samples are shown in the blot. Data shown are the average of three individual mice with standard deviations. The (dysferlin$^{sjl/+}$: Large$^{myd/+}$), (dysferlin$^{sjl/sjl}$: Large$^{myd/+}$), (dysferlin$^{sjl/+}$: Large$^{myd/myd}$), (dysferlin$^{sjl/sjl}$: Large$^{myd/myd}$), and (dysferlin$^{+/+}$: Large$^{myd/myd}$) mice are abbreviated as (sjl/+: myd/+), (sjl/sjl: myd/+), (sjl/+: myd/myd), (sjl/sjl: myd/myd), and (+/+: myd/myd), respectively.
doi:10.1371/journal.pone.0106721.g006

muscle contractions. However, such presumable membrane fragility may be protected in part by the dysferlin functions.

It is known that dysferlin plays a role in membrane repair pathway and several proteins are known to interact with dysferlin, suggesting that dysferlin forms a protein complex during the membrane repair process. MG53 has been shown to interact with dysferlin and participate in membrane repair, and genetic disruption of MG53 in mice results in muscular dystrophy [22]. Caveolin-3 is known to interact with dysferlin and MG53 [31,35]. In the present study, however, we did not observe compensatory upregulation of these proteins in fukutin$^{Hp/−}$ mice, suggesting that dysferlin functions other than membrane repair may play protective roles in the fukutin$^{Hp/−}$ mice. Recently, accumulating evidence has suggested new dysferlin roles other than membrane repair, such as T-tubule formation, maintenance, and stabilizing stress-induced Ca^{2+} signaling [36,37]. In addition, it has been reported that dysferlin deficiency leads to increased expression of complement factors and that complement-mediated muscle injury is associated with the pathogenesis of dysferlin-deficient muscular dystrophy [38]. Therefore, it is possible that such impairments independently or synergically contribute to the pathology of the double mutant mice.

Our results showed, rather unexpectedly, that the double-mutant (dysferlin$^{sjl/sjl}$: Large$^{myd/myd}$) mice did not exhibit significant deterioration of muscle pathology compared with the single-mutant (dysferlin$^{sjl/+}$: Large$^{myd/myd}$) mice. These data suggest that the protective effects of dysferlin in Large$^{myd/myd}$ mice were slightly or much reduced compared with those in fukutin$^{Hp/−}$ mice. Since Large$^{myd/myd}$ mice showed severe and rapid progressive pathology while fukutin$^{Hp/−}$ mice were asymptomatic, our data suggest that the protective effect of dysferlin may be less when disease pathology is advanced and/or severe. It has been reported that a double mutant of dysferlin and dystrophin produced a more exacerbated phenotype than did either single mutant [39]. In our colony, Large$^{myd/myd}$ mice show much more severe and rapid progressive pathology than do dystrophin-deficient mdx mice, supporting our hypothesis of a limited protective effect of dysferlin in dystrophic pathology. Interestingly, the (dysferlin$^{sjl/sjl}$: Large$^{myd/myd}$) mice, however, showed a significantly worse phenotype that did the (dysferlin$^{+/+}$: Large$^{myd/myd}$) mice. In addition, there is a tendency toward a worse phenotype in the order of dysferlin amount, i.e. (dysferlin$^{+/+}$: Large$^{myd/myd}$), (dysferlin$^{sjl/+}$: Large$^{myd/myd}$), and (dysferlin$^{sjl/sjl}$: Large$^{myd/myd}$). These data support the possibility that the protective effect of dysferlin is present even in the severe dystrophic Large$^{myd/myd}$ mice. We conclude that dysferlin has the potential to protect muscular dystrophy progression; however, its effect may depend on disease severity and the amount/activity of dysferlin proteins.

Recently, we showed that the retrotransposal insertion in the 3′-UTR region of fukutin causes abnormal mRNA splicing, which is induced by a strong splice acceptor site in SVA and a rare alternative donor site in the last exon, to produce an aberrantly spliced fukutin protein [7]. The introduction of antisense oligonucleotides that target the splice acceptor, the predicted exonic splicing enhancer, and the intronic splicing enhancer prevented the pathogenic exon trapping by SVA in the cells of

FCMD patients as well as model mice (fukutin$^{Hp/Hp}$ and fukutin$^{Hp/−}$) [7]. This therapeutic strategy can potentially be applied to almost all FCMD patients in Japan, and can therefore be the first radical clinical treatment for dystroglycanopathies. However, there was no animal model to test the effectiveness of the antisense oligonucleotide therapy. Since fukutin$^{Hp/−}$ mice do not exhibit any signs of muscular dystrophy [23], they are not a great model for examining therapeutic effects of this strategy. Skeletal muscle-selective fukutin cKO mice, MCK-fukutin-cKO and Myf5-fukutin-cKO, showed dystrophic pathology [24], but they do not possess the retrotransposal insertion, and thus they are not applicable for testing the antisense oligonucleotide therapy. Our present study demonstrates more severe dystrophic phenotype of (dysferlin$^{sjl/sjl}$: fukutin$^{Hp/−}$) mice compared with (dysferlin$^{sjl/sjl}$: fukutin$^{Hp/+}$) mice. Since the (dysferlin$^{sjl/sjl}$: fukutin$^{Hp/−}$) mice possess the retrotransposal insertion and show dystrophic phenotype, they will be used as the first model for evaluation of the antisense oligonucleotide therapy for FCMD. There is a possibility that the absence of dysferlin could add hurdles on how to interpret the results of the antisense oligonucleotide treatments; however, our quantitative assessments established in this study could overcome this issue. For example, macrophage infiltration (Fig. 4B), connective tissue infiltration (Fig. 4D), and membrane fragility in quadriceps muscles (Fig. 5B) were significantly increased only in the (dysferlin$^{sjl/sjl}$: fukutin$^{Hp/−}$) mice. These parameters in the (dysferlin$^{sjl/sjl}$: fukutin$^{Hp/+}$) mice were not changed compared with those in the (dysferlin$^{sjl/+}$: fukutin$^{Hp/+}$) and the (dysferlin$^{sjl/+}$: fukutin$^{Hp/−}$) mice, and therefore can be used for quantitative evaluation for therapeutic effects of the antisense oligonucleotide treatments. We hope that generation of this novel FCMD model and establishment of the quantitative evaluation for disease severity will accelerate the future translational researches to overcome FCMD.

Supporting Information

Figure S1 Expression of dysferlin and dysferlin-interacting proteins in fukutin$^{Hp/−}$ mice. (A) Western blot analysis of dysferlin, caveolin-3, and MG53 in skeletal muscle extracts from fukutin-deficient fukutin$^{Hp/−}$ (Hp/−), and control fukutin$^{Hp/+}$ (Hp/+) mice. A representative two individual samples for each mouse line are shown in the blots. (B) Quantification of protein expression (panel A) was shown in graphs. Data shown are the average with standard deviations (n = 4 for dysferlin, n = 3 for caveolin-3 and MG53). (C) Immunofluorescence analysis of dysferlin in fukutin$^{Hp/−}$ (Hp/−) and fukutin$^{Hp/+}$ (Hp/+) mice. Bar, 50 µm.
(DOCX)

Acknowledgments

Author Contributions

Conceived and designed the experiments: MK ZL TT. Performed the experiments: MK ZL CI KM. Analyzed the data: MK CI. Contributed reagents/materials/analysis tools: CM KM. Contributed to the writing of the manuscript: MK TT.

References

1. Davies KE, Nowak KJ (2006) Molecular mechanisms of muscular dystrophies: old and new players. Nat Rev Mol Cell Biol 7: 762–773.
2. Barresi R, Campbell KP (2006) Dystroglycan: from biosynthesis to pathogenesis of human disease. J Cell Sci 119: 199–207.
3. Michele DE, Barresi R, Kanagawa M, Saito F, Cohn RD, et al. (2002) Post-translational disruption of dystroglycan-ligand interactions in congenital muscular dystrophies. Nature 418: 417–422.
4. Yoshida-Moriguchi T, Yu L, Stalnaker SH, Davis S, Kunz S, et al. (2010) O-mannosyl phosphorylation of alpha-dystroglycan is required for laminin binding. Science 327: 88–92.
5. Fukuyama Y, Osawa M, Suzuki H (1981) Congenital progressive muscular dystrophy of the Fukuyama type - clinical, genetic and pathological considerations. Brain Dev 3: 1–29.
6. Kobayashi K, Nakahori Y, Miyake M, Matsumura K, Kondo-Iida E, et al. (1998) An ancient retrotransposal insertion causes Fukuyama-type congenital muscular dystrophy. Nature 394: 388–392.
7. Taniguchi-Ikeda M, Kobayashi K, Kanagawa M, Yu CC, Mori K, et al. (2011) Pathogenic exon-trapping by SVA retrotransposon and rescue in Fukuyama muscular dystrophy. Nature 478: 127–131.
8. Godfrey C, Clement E, Mein R, Brockington M, Smith J, et al. (2007) Refining genotype phenotype correlations in muscular dystrophies with defective glycosylation of dystroglycan. Brain 130: 2725–2735.
9. Wells L (2013) The O-Mannosylation Pathway: Glycosyltransferases and Proteins Implicated in Congenital Muscular Dystrophy. J Biol Chem 288: 6930–6935.
10. Vuillaumier-Barrot S, Bouchet-Séraphin C, Chelbi M, Devisme L, Quentin S, et al. (2012) Identification of mutations in TMEM5 and ISPD as a cause of severe cobblestone lissencephaly. Am J Hum Genet 91: 1135–1143.
11. Jae LT, Raaben M, Riemersma M, van Beusekom E, Blomen VA, et al. (2013) Deciphering the glycosylome of dystroglycanopathies using haploid screens for lassa virus entry. Science 340: 479–483.
12. Buysse K, Riemersma M, Powell G, van Reeuwijk J, Chitayat D, et al. (2013) Missense mutations in β-1,3-N-acetylglucosaminyltransferase 1 (B3GNT1) cause Walker-Warburg syndrome. Hum Mol Genet 22: 1746–1754.
13. Stevens E, Carss KJ, Cirak S, Foley AR, Torelli S, et al. (2013) Mutations in B3GALNT2 cause congenital muscular dystrophy and hypoglycosylation of α-dystroglycan. Am J Hum Genet 92: 354–365.
14. Carss KJ, Stevens E, Foley AR, Cirak S, Riemersma M, et al. (2013) Mutations in GDP-mannose pyrophosphorylase B cause congenital and limb-girdle muscular dystrophies associated with hypoglycosylation of α-dystroglycan. Am J Hum Genet 93: 29–41.
15. Yoshida A, Kobayashi K, Manya H, Taniguchi K, Kano H, et al. (2001) Muscular dystrophy and neuronal migration disorder caused by mutations in a glycosyltransferase, POMGnT1. Dev Cell 1: 717–724.
16. Manya H, Chiba A, Yoshida A, Wang X, Chiba Y, et al. (2004) Demonstration of mammalian protein O-mannosyltransferase activity: coexpression of POMT1 and POMT2 required for enzymatic activity. Proc Natl Acad Sci USA 101: 500–505.
17. Inamori K, Yoshida-Moriguchi T, Hara Y, Anderson ME, Yu L, et al. (2012) Dystroglycan function requires xylosyl- and glucuronyltransferase activities of LARGE. Science 335: 93–96.
18. Yoshida-Moriguchi T, Willer T, Anderson ME, Venzke D, Whyte T, et al. (2013) SGK196 Is a Glycosylation-Specific O-Mannose Kinase Required for Dystroglycan Function. Science 341: 896–899.
19. Kuga A, Kanagawa M, Sudo A, Chan YM, Tajiri M, et al. (2012) Absence of post-phosphoryl modification in dystroglycanopathy mouse models and wild-type tissues expressing non-laminin binding form of α-dystroglycan. J Biol Chem 287: 9560–9567.
20. Mariano A, Henning A, Han R (2013) Dysferlin-deficient muscular dystrophy and innate immune activation. FEBS J 280: 4165–4176.
21. Bansal D, Miyake K, Vogel SS, Groh S, Chen CC, et al. (2003) Defective membrane repair in dysferlin-deficient muscular dystrophy. Nature 423: 168–172.
22. Cai C, Masumiya H, Weisleder N, Matsuda N, Nishi M, et al. (2009) MG53 nucleates assembly of cell membrane repair machinery. Nat Cell Biol 11: 56–64.
23. Kanagawa M, Nishimoto A, Chiyonobu T, Takeda S, Miyagoe-Suzuki Y, et al. (2009) Residual laminin-binding activity and enhanced dystroglycan glycosylation by LARGE in novel model mice to dystroglycanopathy. Hum Mol Genet 18: 621–631.
24. Kanagawa M, Yu CC, Ito C, Fukada S, Hozoji-Inada M, et al. (2013) Impaired viability of muscle precursor cells in muscular dystrophy with glycosylation defects and amelioration of its severe phenotype by limited gene expression. Hum Mol Genet 22: 3003–3015.
25. Bittner RE, Anderson LV, Burkhardt E, Bashir R, Vafiadaki E, et al. (1999) Dysferlin deletion in SJL mice (SJL-Dysf) defines a natural model for limb girdle muscular dystrophy 2B. Nat Genet 23: 141–142.
26. Kurahashi H, Taniguchi M, Meno C, Taniguchi Y, Takeda S, et al. (2005) Basement membrane fragility underlies embryonic lethality in fukutin-null mice. Neurobiol Dis 19: 208–217.
27. Grewal PK, Holzfeind PJ, Bittner RE, Hewitt JE (2001) Mutant glycosyltransferase and altered glycosylation of alpha-dystroglycan in the myodystrophy mouse. Nat Genet 28: 151–154.
28. Holzfeind PJ, Grewal PK, Reitsamer HA, Kechvar J, Lassmann H, et al. (2002) Skeletal, cardiac and tongue muscle pathology, defective retinal transmission, and neuronal migration defects in the Large(myd) mouse defines a natural model for glycosylation-deficient muscle-eye-brain disorders. Hum Mol Genet 11: 2673–2687.
29. Han R, Kanagawa M, Yoshida-Moriguchi T, Rader EP, Ng RA, et al. (2009) Basal lamina strengthens cell membrane integrity via the laminin G domain-binding motif of alpha-dystroglycan. Proc Natl Acad Sci USA 106: 12573–12579.
30. Straub V, Rafael JA, Chamberlain JS, Campbell KP (1997) Animal models for muscular dystrophy show different patterns of sarcolemmal disruption. J Cell Biol 139: 375–385.
31. Matsuda C, Hayashi YK, Ogawa M, Aoki M, Murayama K, et al. (2001) The sarcolemmal proteins dysferlin and caveolin-3 interact in skeletal muscle. Hum Mol Genet 10: 1761–1766.
32. Chan YM, Keramaris-Vrantsis E, Lidov HG, Norton JH, Zinchenko N, et al. (2010) Fukutin-related protein is essential for mouse muscle, brain and eye development and mutation recapitulates the wide clinical spectrums of dystroglycanopathies. Hum Mol Genet 19: 3995–4006.
33. Wang CH, Chan YM, Tang RH, Xiao B, Lu P, et al. (2011) Post-natal knockdown of fukutin-related protein expression in muscle by long-term RNA interference induces dystrophic pathology. Am J Pathol 178: 261–272.
34. Murakami T, Hayashi YK, Noguchi S, Ogawa M, Nonaka I, et al. (2006) Fukutin gene mutations cause dilated cardiomyopathy with minimal muscle weakness. Ann Neurol 60: 597–602.
35. Cai C, Weisleder N, Ko JK, Komazaki S, Sunada Y, et al. (2009) Membrane repair defects in muscular dystrophy are linked to altered interaction between MG53, caveolin-3, and dysferlin. J Biol Chem 284: 15894–15902.
36. Klinge L, Harris J, Sewry C, Charlton R, Anderson L, et al. (2010) Dysferlin associates with the developing T-tubule system in rodent and human skeletal muscle. Muscle Nerve 41: 166–173.
37. Kerr JP, Ziman AP, Mueller AL, Muriel JM, Kleinhans-Welte E, et al. (2013) Dysferlin stabilizes stress-induced Ca^{2+} signaling in the transverse tubule membrane. Proc Natl Acad Sci USA 110: 20831–20836.
38. Han R, Frett EM, Levy JR, Rader EP, Lueck JD, et al. (2010) Genetic ablation of complement C3 attenuates muscle pathology in dysferlin-deficient mice. J Clin Invest 120: 4366–4374.
39. Han R, Rader EP, Levy JR, Bansal D, Campbell KP (2011) Dystrophin deficiency exacerbates skeletal muscle pathology in dysferlin-null mice. Skelet Muscle 1: 35.

— 94 —

RESEARCH

Open Access

Japanese founder duplications/triplications involving *BHLHA9* are associated with split-hand/foot malformation with or without long bone deficiency and Gollop-Wolfgang complex

Eiko Nagata[1†], Hiroki Kano[2†], Fumiko Kato[1], Rie Yamaguchi[1], Shinichi Nakashima[1], Shinichiro Takayama[3], Rika Kosaki[4], Hidefumi Tonoki[5], Seiji Mizuno[6], Satoshi Watanabe[7], Koh-ichiro Yoshiura[7], Tomoki Kosho[8], Tomonobu Hasegawa[9], Mamori Kimizuka[10], Atsushi Suzuki[11], Kenji Shimizu[11], Hirofumi Ohashi[11], Nobuhiko Haga[12], Hironao Numabe[13], Emiko Horii[14], Toshiro Nagai[15], Hiroshi Yoshihashi[16], Gen Nishimura[17], Tatsushi Toda[18], Shuji Takada[19], Shigetoshi Yokoyama[19,22], Hiroshi Asahara[19,20], Shinichiro Sano[1,21], Maki Fukami[21], Shiro Ikegawa[2] and Tsutomu Ogata[1*]

Abstract

Background: Limb malformations are rare disorders with high genetic heterogeneity. Although multiple genes/loci have been identified in limb malformations, underlying genetic factors still remain to be determined in most patients.

Methods: This study consisted of 51 Japanese families with split-hand/foot malformation (SHFM), SHFM with long bone deficiency (SHFLD) usually affecting the tibia, or Gollop-Wolfgang complex (GWC) characterized by SHFM and femoral bifurcation. Genetic studies included genomewide array comparative genomic hybridization and exome sequencing, together with standard molecular analyses.

Results: We identified duplications/triplications of a 210,050 bp segment containing *BHLHA9* in 29 SHFM patients, 11 SHFLD patients, two GWC patients, and 22 clinically normal relatives from 27 of the 51 families examined, as well as in 2 of 1,000 Japanese controls. Families with SHFLD- and/or GWC-positive patients were more frequent in triplications than in duplications. The fusion point was identical in all the duplications/triplications and was associated with a 4 bp microhomology. There was no sequence homology around the two breakpoints, whereas rearrangement-associated motifs were abundant around one breakpoint. The rs3951819-*D17S1174* haplotype patterns were variable on the duplicated/triplicated segments. No discernible genetic alteration specific to patients was detected within or around *BHLHA9*, in the known causative SHFM genes, or in the exome.

(Continued on next page)

* Correspondence: tomogata@hama-med.ac.jp
†Equal contributors
¹Department of Pediatrics, Hamamatsu University School of Medicine,
Hamamatsu 431-3192, Japan
Full list of author information is available at the end of the article